nuses, transfer function changes most likely resulted from the PBG-induced BJ reflex.

In conclusion, intravenous PBG administration attenuated the total loop transfer function of the arterial baroreflex, mainly because of the reduction of dynamic gain in the neural arc transfer function. Excess activation of the BJ reflex during acute myocardial ischemia or infarction might exert adverse effects on AP regulation, not only through sympathetic suppression but also through attenuation of baroreflex dynamic gain.

This study was supported by Research Grants for Cardiovascular Diseases (9C-1, 11C-3, and 11C-7) from the Ministry of Health and Welfare of Japan, by Health and Labour Sciences Research Grant for Research on Advanced Medical Technology (H14-Nano-002) from the Ministry of Health, Labour and Welfare of Japan, by a Ground-Based Research Grant for Space Utilization promoted by the National Space Development Agency of Japan and the Japan Space Forum, by Grants-in-Aid for Scientific Research (B-11694337, C-11680862, and C-11670730), and Grants-in-Aid for Encouragement of Young Scientists (13770378) from the Ministry of Education, Science, Sports and Culture of Japan, by Research and Development for Applying Advanced Computational Science and Technology from the Japan Science and Technology, and by the Program for Promotion of Fundamental Studies in Health Science from the Organization for Pharmaceutical Safety and Research.

REFERENCES

1. **Andresen MC and Kunze DL.** Ionic sensitivity of baroreceptors. *Circ Res* 61, *Suppl* I: I-66–I-71, 1987.
2. **Bezold A and Hirt L.** Uber die physiologischen Wirkungen des essingsauren Veratrins. *Unters Physiol Lab Wurtzburg* 1: 75–156, 1867.
3. **Chen HI.** Interaction between the baroreceptor and Bezold-Jarisch reflexes. *Am J Physiol Heart Circ Physiol* 237: H655–H661, 1979.
4. **Glantz SA.** *Primer of Biostatistics* (4th ed.). New York: McGraw-Hill, 1997.
5. **Hosomi H, Katsuda S, Morita H, Nishida Y, and Koyama S.** Interactions among reflex compensatory systems for posthemorrhage hypotension. *Am J Physiol Heart Circ Physiol* 250: H944–H953, 1986.
6. **Ikeda Y, Kawada T, Sugimachi M, Kawaguchi O, Shishido T, Sato T, Miyano H, Matsuura W, Alexander J Jr, and Sunagawa K.** Neural arc of baroreflex optimizes dynamic pressure regulation in achieving both stability and quickness. *Am J Physiol Heart Circ Physiol* 271: H882–H890, 1996.
7. **Jarisch A and Richter H.** Die afferenten Bahnen des Veratrineeffekts in den Herznerven. *Arch Exp Pathol Pharmacol* 193: 355–371, 1939.
8. **Kashihara K, Takahashi Y, Chatani K, Kawada T, Zheng C, Li M, Sugimachi M, and Sunagawa K.** Intravenous angiotensin II does not affect dynamic baroreflex characteristics of the neural or peripheral arc. *Jpn J Physiol.* In press.
9. **Kawada T, Sato T, Shishido T, Inagaki M, Tatewaki T, Yanagiya Y, Sugimachi M, and Sunagawa K.** Summation of dynamic transfer characteristics of left and right carotid sinus baroreflexes in rabbits. *Am J Physiol Heart Circ Physiol* 277: H857–H865, 1999.
10. **Kawada T, Shishido T, Inagaki M, Tatewaki T, Zheng C, Yanagiya Y, Sugimachi M, and Sunagawa K.** Differential dynamic baroreflex regulation of cardiac and renal sympathetic nerve activities. *Am J Physiol Heart Circ Physiol* 280: H1581–H1590, 2001.
11. **Kawada T, Yamazaki T, Akiyama T, Sato T, Shishido T, Inagaki M, Takaki H, Sugimachi M, and Sunagawa K.** Differential acetylcholine release mechanisms in the ischemic and non-ischemic myocardium. *J Mol Cell Cardiol* 32: 405–414, 2000.
12. **Kawada T, Yamazaki T, Akiyama T, Shishido T, Inagaki M, Uemura K, Miyamoto T, Sugimachi M, Takaki H, and Sunagawa K.** In vivo assessment of acetylcholine-releasing function at cardiac vagal nerve terminals. *Am J Physiol Heart Circ Physiol* 281: H139–H145, 2001.
13. **Kawada T, Yanagiya Y, Uemura K, Miyamoto T, Zheng C, Li M, Sugimachi M, Sunagawa K.** Input-size dependence of the baroreflex neural arc transfer characteristics. *Am J Physiol Heart Circ Physiol* 284: H404–H415, 2003.
14. **Kawada T, Zheng C, Yanagiya Y, Uemura K, Miyamoto T, Inagaki M, Shishido T, Sugimachi M, and Sunagawa K.** High-cut characteristics of the baroreflex neural arc preserve baroreflex gain against pulsatile pressure. *Am J Physiol Heart Circ Physiol* 282: H1149–H1156, 2002.
15. **Levison WH, Barnett GO, and Jackson WD.** Nonlinear analysis of the baroreceptor reflex system. *Circ Res* 18: 673–682, 1966.
16. **Mark AL.** The Bezold-Jarisch reflex revisited: clinical implications of inhibitory reflexes originating in the heart. *J Am Coll Cardiol* 1: 90–102, 1983.
17. **Marmarelis PZ and Marmarelis VZ.** The white noise method in system identification. In: *Analysis of Physiological Systems.* New York: Plenum, 1978, p. 131–221.
18. **Merahi N, Orer HS, Laporte AM, Gozlan H, Hamon M, and Laguzzi R.** Baroreceptor reflex inhibition induced by the stimulation of serotonin 3 receptors in the nucleus tractus solitarius of the rat. *Neuroscience* 46: 91–100, 1992.
19. **Meyrelles SS, Bernardes CF, Modolo RP, Mill JG, and Vasquez EC.** Bezold-Jarisch reflex in myocardial infarcted rats. *J Auton Nerv Syst* 63: 144–152, 1997.
20. **Meyrelles SS, Mill JG, Cabral AM, and Vasquez EC.** Cardiac baroreflex properties in myocardial infarcted rats. *J Auton Nerv Syst* 60: 163–168, 1996.
21. **Milhorn HT.** Static characteristics of technological and physiological control systems. In: *The Application of Control Theory to Physiological Systems.* Philadelphia, PA: Saunders, 1966, p. 156–166.
22. **Mohrman DE and Heller LJ.** *Cardiovascular Physiol* (4th ed.). New York: McGraw-Hill, 1997, p. 151-173.
23. **Pires JG, Silva SR, Ramage AG, and Futuro-Neto HA.** Evidence that 5-HT3 receptors in the nucleus tractus solitarius and other brainstem areas modulate the vagal bradycardia evoked by activation of the von Bezold-Jarisch reflex in the anesthetized rat. *Brain Res* 791: 229–234, 1998.
24. **Robertson D, Hollister AS, Forman MB, and Robertson RM.** Reflexes unique to myocardial ischemia and infarction. *J Am Coll Cardiol* 5: 99B–104B, 1985.
25. **Sato T, Kawada T, Inagaki M, Shishido T, Takaki H, Sugimachi M, and Sunagawa K.** New analytic framework for understanding the sympathetic baroreflex control of arterial pressure. *Am J Physiol Heart Circ Physiol* 276: H2251–H2261, 1999.
26. **Sato T, Kawada T, Shishido T, Miyano H, Inagaki M, Miyashita H, Sugimachi M, Knuepfer MM, and Sunagawa K.** Dynamic transduction properties of in situ baroreceptors of rabbits aortic depressor nerve. *Am J Physiol Heart Circ Physiol* 274: H358–H365, 1998.
27. **Schultz HD.** Cardiac vagal chemosensory afferents. Function in pathophysiological states. *Ann NY Acad Sci* 940: 59–73, 2001.
28. **Suzuki S, Ando S, Imaizumi T, and Takeshita A.** Effects of anesthesia on sympathetic nerve rhythm: power spectral analysis. *J Auton Nerv Syst* 43: 51–58, 1993.
29. **Veelken R, Hilgers KF, Leonard M, Scrogin K, Ruhe J, Mann JF, and Luft FC.** A highly selective cardiorenal serotonergic 5-HT_3-mediated reflex in rats. *Am J Physiol Heart Circ Physiol* 264: H1871–H1877, 1993.
30. **Veelken R, Leonard M, Stetter A, Hilgers KF, Mann JF, Reeh PW, Geiger H, and Luft FC.** Pulmonary serotonin 5-HT_3-sensitive afferent fibers modulate renal sympathetic nerve activity in rats. *Am J Physiol Heart Circ Physiol* 272: H979–H986, 1997.
31. **Verberne AJ and Guyenet PG.** Medullary pathway of the Bezold-Jarisch reflex in the rat. *Am J Physiol Regul Integr Comp Physiol* 263: R1195–R1202, 1992.
32. **Whalen EJ, Johnson AK, and Lewis SJ.** Functional evidence for the rapid desensitization of 5-HT(3) receptors on vagal afferents mediating the Bezold-Jarisch reflex. *Brain Res* 873: 302–305, 2000.

Eur J Appl Physiol (2004) 93: 340–346
DOI 10.1007/s00421-004-1219-x

ORIGINAL ARTICLE

Tadayoshi Miyamoto · Masashi Inagaki
Hiroshi Takaki · Toru Kawada · Yusuke Yanagiya
Masaru Sugimachi · Kenji Sunagawa

Integrated characterization of the human chemoreflex system controlling ventilation, using an equilibrium diagram

Accepted: 26 July 2004 / Published online: 23 September 2004

Abstract The chemoreflex system controlling ventilation consists of two subsystems, i.e., the central controller (controlling element), and peripheral plant (controlled element). We developed an integral framework to quantitatively characterize individual ventilatory regulation by experimental determination of an equilibrium diagram using a modified metabolic hyperbola and the CO_2 response curve. In 13 healthy males, the steady-state arterial CO_2 pressure (P_aCO_2) and minute ventilation ($\dot{V}_E$) were measured. To characterize the central controller, we changed fraction of inspired CO_2 (0, 3.5, 5 and 6% CO_2 in 80% oxygen with nitrogen balance) and measured the P_aCO_2–$\dot{V}_E$ relation. To characterize the peripheral plant, we altered $\dot{V}_E$ by hyper- or hypoventilation using a visual feedback method, which made it possible to control both tidal volume and breathing frequency, and measured the $\dot{V}_E$–P_aCO_2 relation. The intersection between the two relationship lines gives the operating point. The relationship between P_aCO_2 and $\dot{V}_E$ for the central controller was reasonably linear in each subject ($r^2 = 0.808 \sim 0.995$). The peripheral plant approximated a modified metabolic hyperbolic curve ($r^2 = 0.962 \sim 0.996$). The operating points of the system estimated from the two relationship lines were in good agreement with those measured under the closed-loop condition. The gain of the central controller was 1.9 (1.0) l min^{-1} mmHg^{-1} and that of the peripheral plant was 3.0 (0.5) mmHg l^{-1} min^{-1}. The total loop gain, the product of the two gains, was 5.3 (2.5). We conclude that human ventilatory regulation by the respiratory chemoreflex system can be quantitatively characterized using an equilibrium diagram. This framework should be useful for understanding the mechanisms responsible for abnormal ventilation under various pathophysiological conditions.

Keywords Control of breathing · Respiratory system · Chemosensitivity · Metabolic hyperbola · Total loop gain

T. Miyamoto (✉) · M. Inagaki · H. Takaki · T. Kawada
Y. Yanagiya · M. Sugimachi · K. Sunagawa
Department of Cardiovascular Dynamics,
National Cardiovascular Center Research Institute,
5-7-1 Fujishirodai, Suita, 565-8565 Osaka, Japan
E-mail: miyamoto@res.ncvc.go.jp
Tel.: +81-66-8335012
Fax: +81-66-8355403

T. Miyamoto
Japan Association for the Advancement of Medical Equipment,
105-0013 Tokyo, Japan

Y. Yanagiya
The Organization for Pharmaceutical Safety and Research,
100-0013 Tokyo, Japan

Introduction

The chemoreflex is a powerful feedback control system functioning physiologically to maintain respiratory homeostasis. In the presence of normal kidney function, ventilatory regulation keeps arterial CO_2 pressure (P_aCO_2) or pH nearly constant, indicating that P_aCO_2 serves as a controlled variable. The respiratory chemoreflex system consists of two subsystems, i.e., the central controller (controlling element) and peripheral plant (controlled element) (Fig. 1A). In the central controller, the input to the chemoreceptors is P_aCO_2 and the output is minute ventilation ($\dot{V}_E$). Therefore, we can characterize the central controller by observing changes in $\dot{V}_E$ in response to changes in P_aCO_2 (P_aCO_2–$\dot{V}_E$ relation). Conversely, in the peripheral plant, the input is $\dot{V}_E$ and the output is P_aCO_2. Thus, the peripheral plant can be characterized by observing P_aCO_2 in response to changes in $\dot{V}_E$ ($\dot{V}_E$–P_aCO_2 relation). Since both relations share common variables, i.e., $\dot{V}_E$ and P_aCO_2, the resultant operating point of ventilatory response under the closed-loop condition is determined by the intersection of the two relations (Fig. 1B). This is to say that the quantitative analysis of two arcs provides us with a framework by which we can analytically evaluate how the unique value of $\dot{V}_E$ is determined by the respiratory chemoreflex

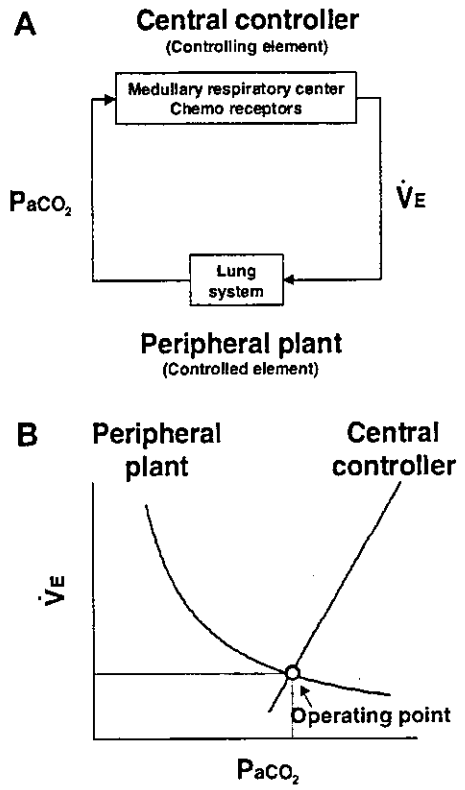

Fig. 1 A The respiratory chemoreflex system consists of two subsystems, the central controller and peripheral plant. B In the central controller the input parameter is arterial CO_2 pressure (P_aCO_2), the output parameter is minute ventilation ($\dot{V}_E$). The central controller can be characterized by observing changes in $\dot{V}_E$ in response to changes in P_aCO_2. In the peripheral plant, input is $\dot{V}_E$, and output is P_aCO_2. The peripheral plant can be characterized by observing changes in P_aCO_2 in response to changes in $\dot{V}_E$. Since both relationships share common variables, the resultant operating point of ventilatory response under the closed-loop condition is determined by the intersection of the two relations

system, how changes in the central controller properties affect $\dot{V}_E$, or how changes in the peripheral plant properties affect $\dot{V}_E$.

Previously, several investigators have shown conceptual frameworks to integrally characterize ventilatory regulation of the respiratory chemoreflex system using equilibrium diagrams (Defares 1964; Cunningham et al. 1986; Folgering 1988; Milhorn 1966). In those studies, the terms for ventilation ($\dot{V}_E$ and dead space) have been eliminated from the metabolic hyperbola equation. Although Loeschcke (1960) experimentally characterized the central controller and peripheral plant as the framework for their analysis, the peripheral plant described the relation between alveolar ventilation ($\dot{V}_A$) and P_aCO_2, whereas the central controller described the P_aCO_2–$\dot{V}_E$ relation. Berger et al. (1977) arithmetically described the diagram for peripheral plant, which expressed the relation between $\dot{V}_E$ and P_aCO_2, assuming that the rate of CO_2 production is fixed, and the dead space (V_D) to tidal volume (V_T) ratio (V_D/V_T) is constant, whereas the V_D/V_T with variation in $\dot{V}_E$ is not fixed in an "actual life" physiological system. Furthermore, almost all studies have failed to consider the modification of the hyperbola equation to take into account the metabolic change due to the work of breathing, which is not insignificant under pathophysiological conditions. Consequently, none of those reports quantitatively validated the integral characterization of the ventilatory regulation of the chemoreflex system.

The purpose of this study was to experimentally establish a framework to analyze the ventilatory regulation of the human respiratory chemoreflex system using an equilibrium diagram. To characterize the peripheral plant ($\dot{V}_E$–P_aCO_2 relation), we altered $\dot{V}_E$ by voluntary hyper- or hypoventilation using a visual feedback method which made it possible to control both V_T and breathing frequency, and thus $\dot{V}_E$ and V_D/V_T with variation in $\dot{V}_E$. To take into account the metabolic change due to the work of breathing, we fitted the $\dot{V}_E$–P_aCO_2 relation to a modified hyperbola equation (Appendix).

Methods

Subjects

Thirteen healthy young males, non-smokers, with no history or evidence of cardiac or pulmonary disease, whose mean age ranged between 18 and 22 years [mean (SD) 21.0 (1.3) years], served as subjects for this study. Their mean body mass and height were 63.8 (6.3) kg and 171.1 (6.3) cm, respectively. The subjects gave their written consent to participate in the study after the possible risks of participation were explained. The experimental protocol and consent form were reviewed and approved by the Human Subjects Committee of National Cardiovascular Center.

Experimental apparatus and measurements

Ventilatory responses were measured using an open-circuit apparatus. The subjects breathed through a face mask attached to a low-resistance one-way valve with a built-in hot-wire flow meter. The valve mechanism allowed subjects to inspire room air or a selected gas mixture from a 200-l plastic bag containing 0.0, 3.5, 5.0 or 6.0% CO_2 in 80% O_2 with N_2 balance. The total instrumental dead space was 200 ml.

Respiratory and metabolic data during the experiments were recorded by an automatic breath-by-breath respiratory gas analyzing system (AE-280S, Minato Medical Science, Osaka, Japan) consisting of a hot-wire flow meter, sampling tube, filter, suction pump, O_2 analyzer made from a zirconium element, and an infrared CO_2 analyzer. We digitized (at 200 Hz) expired flow, CO_2 and O_2 concentrations, and derived V_T, $\dot{V}_E$ and end-tidal CO_2. Flow signals were computed to single breath data, and matched to gas concentrations identified as single breaths using the peak end-tidal CO_2, after

accounting for the time delay in gas concentration measurements. The corresponding O_2 uptake and CO_2 output ($\dot{V}CO_2$) values for each breath were calculated from inspired–expired gas concentration differences, and by expired ventilation, with inspired ventilation being calculated by N_2 correction.

P_aCO_2 and oxygen pressure (PO_2) were measured by using a blood gas analyzer (IL 1620, Instrumentation Laboratory, USA).

Experimental procedure

For 24 h preceding the day of the experiments, we instructed the subjects to avoid strenuous exercise and food with a high salt content. They were required to abstain from consuming food, alcohol or caffeine for 3 h preceding each test. The subjects remained in the fasting state throughout all experimental runs, lasting ~5 h. Before starting the experiment, the subjects rested in a comfortable chair in the sitting position. After local application of 2% lidocaine solution, we positioned a catheter in the brachial artery so that samples of arterial blood could be taken. The experiment started 20–30 min after we positioned the catheter. During experiments, we encouraged subjects to relax by listening to music with a headset and to distract their attention away from the experiment. We provided subjects with a comprehensive explanation of the experimental procedure, but provided little information on the specific purpose of the study. We informed the subjects that CO_2 would be given during the course of the experiment. We instructed them to indicate if the discomfort was such that they wished to end the run.

To minimize the possibility of the so-called dog-leg phenomenon (Cunningham et al. 1986), which is believed to be a function of restlessness, anxiety and discomfort, each experiment lasted for 2 days, with the first day used as a practice session. In the practice session, the subjects underwent the same experiments except for the taking of arterial blood. To characterize central controller and peripheral plant, the subjects underwent two experimental procedures, which consisted of the $\dot{V}_E$ response to hypercapnia and P_aCO_2 response to hypo- and hyperventilation on the same day.

$\dot{V}_E$ response to hypercapnia

The $\dot{V}_E$ response to hypercapnia consisted of four trials [fraction of inspired CO_2 ($FICO_2$) 0.00, 0.035, 0.05, 0.06]. We induced hypercapnia by changing the level of inspired CO_2 concentrations. Each $FICO_2$ trial ran for 15 min at approximately 10–15 min intervals. This duration is long enough to permit CO_2 to reach its new steady-state value at the central chemoreceptors (Honda et al. 1983; Poon and Greene 1985; Pianosi et al. 1994; Teppema et al. 2000). During the interval periods, the subjects inspired room air. The order of the trials was randomized for each subject. We performed all trials under the hyperoxic condition to abolish O_2-sensitive chemoreflex (Ohyabu et al. 1982; Robbins 1988; Mohan and Duffin 1997).

P_aCO_2 response to hypo- and hyperventilation

The P_aCO_2 response to ventilation consisted of four trials (three hyperventilation and one hypoventilation). To avoid the possible effects of different breathing patterns on the $\dot{V}_E$–P_aCO_2 relation, in the hyperventilation trials, both V_T and breathing frequency were altered deliberately by matching the breathing pattern to that during hypercapnia $FICO_2$ trials, while inhaling 0% CO_2 in 80% O_2 with N_2 balance. In the hypoventilation trial, $\dot{V}_E$ was set to 70% of $\dot{V}_E$ during the 0.00 $FICO_2$ trial. The breathing pattern was estimated from the relationships between $\dot{V}_E$ and V_T in each subject. Each trial ran for 15 min with an interval of 10–15 min. The order of the trials was randomized for each subject.

During hypo- and hyperventilation trials, the inspired and expired volume curves were continuously displayed on a screen monitor. We constructed a sinusoidal command wave from the breathing pattern of the subjects during the hypercapnia trials. The sinusoidal command wave was simultaneously displayed on the same screen monitor in each trial. We instructed the subjects to match their volume curve with the sinusoidal command wave. As a result, both the V_T and breathing frequency, and thus $\dot{V}_E$, were precisely controlled by the visual feedback.

Since preliminary measurements indicated that P_aCO_2 response to $\dot{V}_E$ and $\dot{V}_E$ response to P_aCO_2 reached steady states in 8–12 min, we represented each response by averaging it in the last 3 min. The arterial blood samples (2.5 ml) were collected at minutes 12.5, 13.5, and 14.5 of each trial period. A 3-point average value for each trial was computed as the steady-state value. The measured values of operating points in the subjects were defined to be the steady-state values for $\dot{V}_E$ and P_aCO_2 that were obtained during the 0.00 $FICO_2$ trial without visual feedback (during spontaneous breathing).

Data analysis

To characterize the central controller, we used a conventional linear equation, $\dot{V}_E = S(P_aCO_2 - B)$, and determined the slope S and intercept B using a standard least-squares regression method. To characterize the peripheral plant, we modified the metabolic hyperbola as $P_aCO_2 = A/\dot{V}_E + C$ in which CO_2 production by respiration was taken into consideration (Appendix). We derived the values of A and C by a standard least-squares regression method.

Statistical analysis

All values are reported as mean (SD). Statistical significance was accepted at $P<0.05$. Pearson product-moment correlations were calculated between $\dot{V}_E$ values and each P_aCO_2. The accuracy of prediction was assessed by standard error of estimate (SEE).

Results

Shown in the left panels of Fig. 2 are diagrams of characteristics of peripheral controller and central plant derived from a representative subject. The right panels show pooled data from all subjects. As shown in Fig. 2A, $\dot{V}_E$ increased linearly with P_aCO_2 both in a representative case and in pooled data ($r^2=0.808\sim0.995$ in each subject). The slope of the regression line for pooled data, which represents the gain of the central controller, was 1.9 (1.0) l min^{-1} mmHg^{-1}, and the intercept was 31.5 (5.1) mmHg. The effect of changes in $\dot{V}_E$ on P_aCO_2 is shown in Fig. 2B. The relationship approximated a modified metabolic hyperbola reasonably well ($r^2=0.962\sim0.996$ in each subject). The mean value of the numerator of the parabola was 331.3 (80.3) l min^{-1} mmHg^{-1} with an asymptote of 9.0 (2.2) mmHg.

Since we can characterize both the central controller and peripheral plant with the common variables of $\dot{V}_E$ and P_aCO_2, the operating point is determined as the

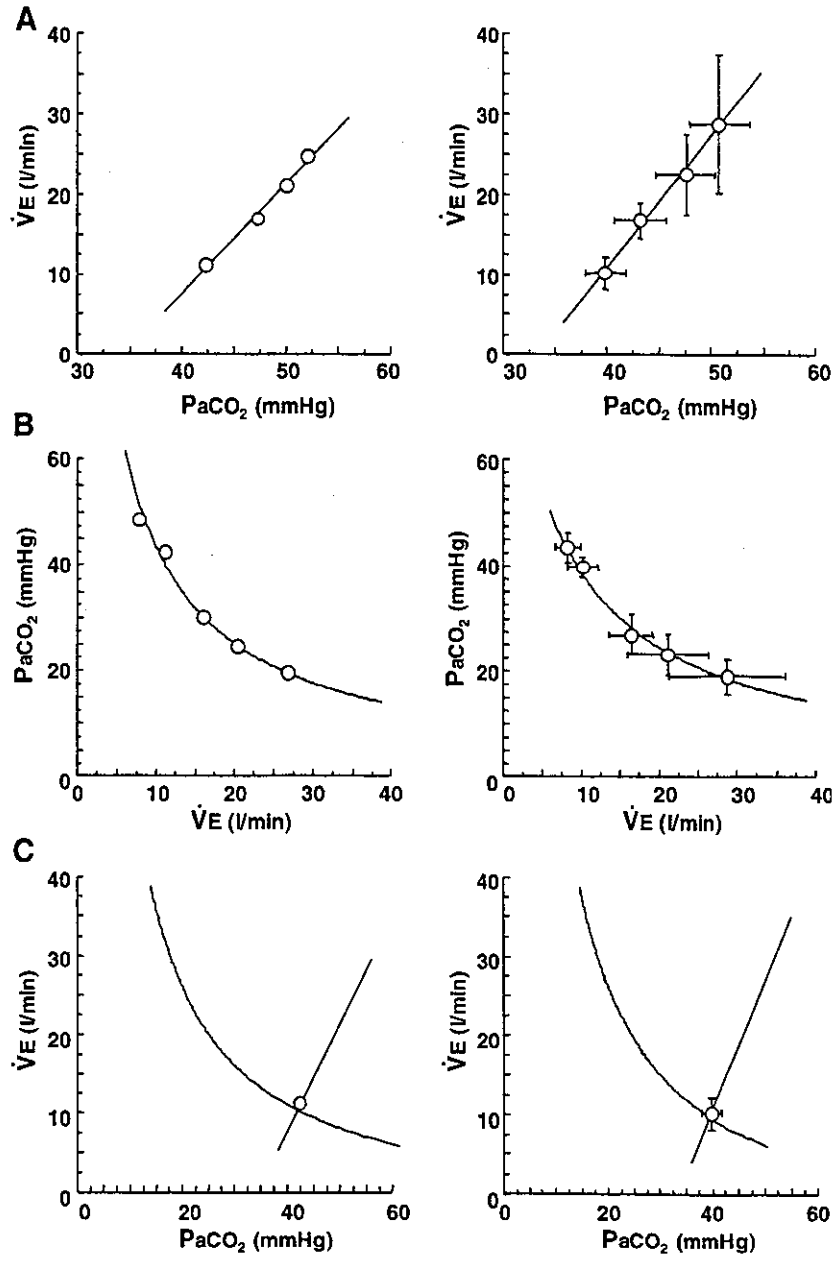

Fig. 2 A, B Characteristics of central controller, peripheral plant and equilibrium diagram derived from a representative case (*left panels*) and pooled data from all subjects (*right panels*). *Vertical bars* indicate SD. **A** $\dot{V}_E$ linearly increased with P_aCO_2 in a representative case and in pooled data ($r^2=0.812\sim0.994$ in each subject). The averaged regression line was $\dot{V}_E=1.7$ ($P_aCO_2-31.5$). **B** The peripheral plant was characterized by a modified metabolic hyperbola. The modified hyperbola fitted a representative case well (*left panel*), and also the pooled data ($r^2=0.927\sim0.995$ in each subject). The best-fit hyperbola for pooled data was $P_aCO_2=294.1/\dot{V}_E+9.2$. **C** The operating points estimated by the equilibrium diagram were very close to those measured (*open circle*) both in a representative case and in pooled data

intersection between the two operational lines. As shown in Fig. 2C, the operating points estimated by the equilibrium diagram (the intersection between the two relationship lines) were very close to those during closed-loop spontaneous breathing (open circles) in a representative subject. This is further supported by the fact that in the pooled data, the estimated P_aCO_2 and $\dot{V}_E$ values at the operating point were indistinguishable from the measured values [39.2 (2.1) vs 39.9 (1.9) mmHg, and 9.9 (1.8) vs 10.2 (2.0) l min^{-1}, respectively]. The gain of the peripheral plant estimated by the reciprocal of the slope of the hyperbola curve at the operating point was 3.0 (0.5) mmHg l^{-1} min^{-1}. The estimated total loop gain at the operating point, i.e., the product of the gains of the central controller and the peripheral plant, was 5.3 (2.5).

The relationships between the values of the operating points estimated by the equilibrium diagram and the measured values are illustrated in Fig. 3. The estimated P_aCO_2 was tightly correlated with measured P_aCO_2 ($y=0.85x+0.86$, $r^2=0.851$, SEE = 0.84, $P<0.001$). Similarly, the estimated $\dot{V}_E$ was tightly correlated with measured $\dot{V}_E$ ($y=1.02x+0.02$, $r^2=0.849$, SEE = 0.73, $P<0.001$). Thus, the equilibrium diagram enables us to quantitatively estimate the $\dot{V}_E$ and P_aCO_2 at the operating point.

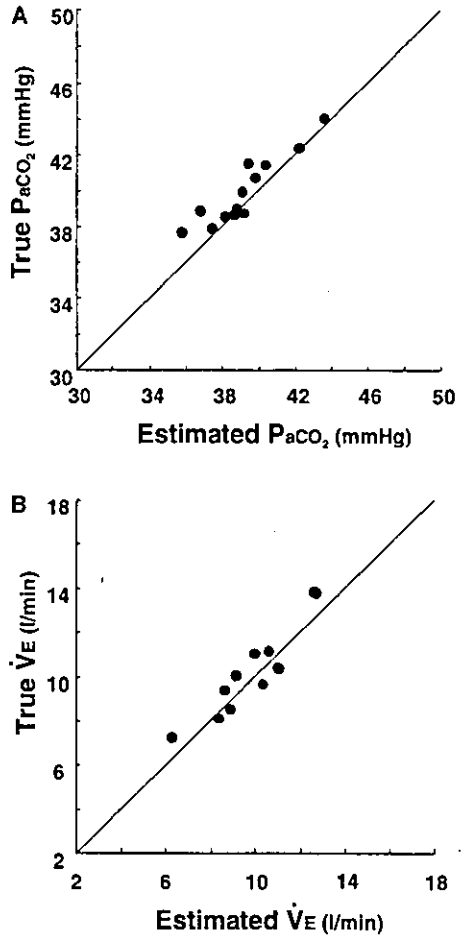

Fig. 3A, B Relationships between the operating points estimated by the equilibrium diagram and those measured. **A** The estimated P_aCO_2 was tightly correlated with measured P_aCO_2 [$y=0.85x+0.86$, $r^2=0.851$, standard error of estimate (SEE) = 0.84, $P<0.001$]. *Continuous line* The line of identity. **B** The estimated $\dot{V}_E$ was tightly correlated with measured $\dot{V}_E$ ($y=1.02x+0.02$, $r^2=0.849$, SEE = 0.73, $P<0.001$). *Continuous line* The line of identity

Discussion

We have shown that the framework obtained by using the equilibrium diagram and by breaking down the chemoreflex respiratory feedback system into the central controller and peripheral plant enabled us to evaluate how the $\dot{V}_E$ and P_aCO_2 are determined under the closed-loop condition. The major findings include:

1. We quantitatively identified the characteristics of both central controller and peripheral plant for the respiratory chemoreflex system controlling ventilation in humans, using an equilibrium diagram
2. We demonstrated that the operating points of the chemoreflex system estimated from both the open-loop operational lines were in good agreement with those measured under the closed-loop condition
3. Central controller gain was 1.9 (1.0) l min^{-1} $mmHg^{-1}$, the peripheral plant gain was 3.0 (0.5) mmHg l^{-1} min^{-1}, and the total loop gain, the product of two gains, was 5.3 (2.5)

Significance of equilibrium diagram in analyzing chemoreflex respiratory feedback regulation

In feedback control systems, system properties that determine the operating point cannot be elucidated unless the feedback loop is open. That is why we opened the feedback loop and determined subsystem open-loop properties using common variables between the two subsystems, i.e., P_aCO_2 and $\dot{V}_E$. Once the open-loop properties are characterized, the resultant operating point is determined as the intersection between the two functional lines (Defares 1964; Milhorn 1966; Cunningham et al. 1986). The fact that the estimated P_aCO_2 and $\dot{V}_E$ agreed well with those measured under the closed-loop condition (Fig. 3) suggested that two subsystems are mutually independent and the open-loop characteristics truly represent subsystem properties, thereby validating our framework of using an equilibrium diagram to analyze chemoreflex respiratory regulation.

Respiratory homeostasis is maintained by a powerful feedback control system mediated by P_aCO_2. The magnitude of this controlling power can be expressed as the "total loop gain" (Berger et al. 1977; Honda et al. 1983; Khoo 2000). The concept of the total loop gain is widely used in control theory. Based on our framework using an equilibrium diagram analysis, we found that the

gain at the operating point of the central controller was 1.9 l min^{-1} $mmHg^{-1}$ and that of the peripheral plant was 3.0 mmHg l^{-1} min^{-1}. The total loop gain, the product of the two gains, was 5.3. According to feedback control theory, the magnitude of attenuation is quantitatively derived as 1/(total loop gain + 1). Therefore, when a 10 mmHg of P_aCO_2 disturbance is introduced into the system, the resultant change in P_aCO_2 is only 1.5 mmHg, suggesting that the chemoreflex is a very powerful mechanism for stabilizing P_aCO_2.

Reported values of total loop gain range from 10 to 20, or 2–4 times larger than values we found in our experiments (Milhorn 1966; Berger et al. 1977; Honda et al. 1983). In all these studies, the P_aCO_2 response to $\dot{V}_A$ (or $\dot{V}_E$) was fitted to a so-called metabolic hyperbola where the O_2 consumption of respiratory muscle was ignored. The increase in work of breathing could lead to an overestimation of the peripheral plant gain at the same operating point. This is likely to be a reason why we had a lower total loop gain than previously reported. Previous studies estimated the total loop gain without opening each of the subsystems in the feedback loop. This might introduce an additional bias in estimating the total loop gain. The fact that a modified hyperbola fits better than the original hyperbola suggests that our estimated gain is likely to be more accurate (Appendix).

Quantitative analysis of central controller and peripheral plant in humans

Many factors affect the characteristics of the peripheral plant and its gain at the operating point. If O_2 consumption is increased, as it is during exercise, it shifts the parabolic $\dot{V}_E$ response to P_aCO_2 upward depending upon the metabolic rate. As a result, the value of the numerator of the parabola increases (Appendix, Eq. 3). Various pathological conditions also shift the parabola upward. Changes in respiration patterns alone from slow–deep to rapid–shallow breathing inevitably increase physiological dead-space, thereby increasing P_aCO_2 for a given $\dot{V}_E$. This results in an upward shift of the parabola. If tachypnea by itself increases O_2 consumption by the respiratory muscle, as is often seen in patients with obstructive pulmonary disease (COPD), the parabola will shift to right, with a larger value for its asymptote (Appendix, Eq. 3). This could cause a smaller gain of the peripheral plant at the operating point in patients with COPD than in healthy subjects. Other pathological conditions that shift the parabola upward include pulmonary interstitial fibrosis and $\dot{V}_A/Q$ mismatch. Once the parabola shifts upward, such as in the above pathophysiological conditions, even if the functioning of the central controller remains normal, both $\dot{V}_E$ and P_aCO_2 should increase under the closed-loop condition.

The sensitivity of $\dot{V}_E$ to P_aCO_2 depends on the characteristics of the central controller. It is well known that narcotics, anesthetics, sedatives or other drugs make it less sensitive (Folgering 1988; Teppema et al. 2000). In this case, P_aCO_2 increases as the result of decreased $\dot{V}_E$ even if the characteristics of the peripheral plant remain unchanged. Conversely, some drugs such as caffeine, almitrine and progesterone increase the sensitivity of the chemoreflex. If they do not alter the characteristics of the peripheral plant, these drugs should decrease P_aCO_2. Indeed, these predictions are consistent with experimental observations (Cummin et al. 1990; Pianosi et al. 1994).

Characteristics of the central controller and peripheral plant may change simultaneously. In patients with heart failure, central controller gain is known to be higher than normal (Javaheri 1999). A typical respiratory pattern in these patients is rapid shallow respiration. Therefore, it is likely that physiological dead space increases, thereby shifting the hyperbola characterizing the peripheral plant upward. As a result, $\dot{V}_E$ increases with lower, normal or higher P_aCO_2 depending upon the degree of coexisting central sensitization. In contrast, patients with COPD have a lower CO_2 sensitivity (Patakas et al. 1978). Since the hyperbola representing the characteristics of the peripheral plant is likely to shift upward, resultant P_aCO_2 and $\dot{V}_E$ would be higher than in the normal population. This is also consistent with experimental observations (Patakas et al. 1978).

Despite numerous investigations, the mechanisms responsible for exercise hyperpnea have not been fully elucidated. According to our framework using the equilibrium diagram, increases in CO_2 production during exercise shift the metabolic hyperbola upward. This is to say that if the characteristics of the central controller remain unaltered, exercise must increase P_aCO_2. However, the fact that P_aCO_2 ordinarily does not change much during exercise (Oren et al. 1981; Dempsey et al. 1984; Poon and Greene 1985; Wasserman et al. 1986; Whipp and Pardy 1986) suggests that exercise concurrently sensitizes the respiratory chemoreflex, thereby keeping P_aCO_2 fairly constant in healthy subjects.

Limitation

We quantitatively identified the characteristics of the peripheral plant using the visual feed back method. The method made it possible to control accurately both the V_T and breathing frequency, and thus $\dot{V}_E$. However, the inspiration and expiration duration during trials were not controlled, because a sinusoidal wave was used as a command curve in this experiment. Therefore, this nonphysiological respiration pattern might affect the P_aCO_2 response to $\dot{V}_E$. Nevertheless, the fact that the estimated values for P_aCO_2 and $\dot{V}_E$ correlated well with those measured suggests that the framework of analysis remains valid in spite of the variability inevitably introduced by the experimental conditions.

Our proposed framework should be useful in understanding the mechanisms responsible for the ventilatory abnormalities seen in patients with chronic heart failure and COPD. However, our method is limited by complicated, time-consuming procedures. For practical application of this framework in clinical settings, it will be necessary to simplify the procedures to characterize the properties of the central controller and peripheral plant.

Conclusion

Human ventilatory regulation by the respiratory chemoreflex feedback system can be quantitatively characterized using an equilibrium diagram. This theoretical framework should be a powerful tool in understanding the mechanism responsible for abnormal ventilation under various pathophysiological conditions.

Acknowledgment This study was supported by the Program for Promotion of Fundamental Studies in Health Science of the Pharmaceuticals and Medical Devices Agency of Japan, by a Health and Labour Sciences Research Grant for Research on Advanced Medical Technology from the Ministry of Health, Labour and Welfare of Japan.

Appendix

The metabolic hyperbola has been described by the following equation:

$$P_aCO_2 = 863(\dot{V}CO_2/\dot{V}_A) \quad (1)$$

where $\dot{V}_A$ is alveolar ventilation (Cunningham et al. 1986; Whipp and Pardy 1986). If we approximate $\dot{V}_A$ by $\dot{V}_E$ and take the metabolic work of respiratory muscles (Harms and Dempsey 1999) into consideration, Eq. 1 can be rewritten as:

$$P_aCO_2 = 863(\alpha + \beta\dot{V}_E)/\dot{V}_E \quad (2)$$

where α is constant and β is a constant representing respiratory work-related CO_2 production. Rearranging Eq. 2 yields:

$$P_aCO_2 = A/\dot{V}_E + C \quad (3)$$

where $A = 863\alpha$ and $C = 863\beta$

We fitted both the original hyperbola (Eq. 1) and modified hyperbola (Eq. 3) to the P_aCO_2 changes in response to changes in $\dot{V}_E$. In each subject, the correlation coefficient was significantly higher ($P < 0.001$) in the modified model than the original model [the mean r^2 values; 0.985 (0.01) vs 0.898 (0.04)]. Therefore, we used the modified hyperbola for our analysis.

References

Berger, AJ, Mitchell, RA, Severinghaus JW (1977) Regulation of respiration (third of three parts). N Engl J Med 297:194–201

Cummin AR, Jacobi MS, Patil CP, Telford RJ, Morgan CN, Saunders KB (1990) The effect of almitrine on the steady-state ventilatory response to carbon dioxide at rest and during exercise in man. Eur Respir J 3:693–698

Cunningham DJC, Robbins PA, Wolff CB (1986) In: Handbook of Physiology. Integration of respiratory responses to changes in alveolar partial pressures of CO_2 and O_2 and in arterial pH. American Physiolological Society, Bethesda, MD, pp 476–528

Defares JG (1964) In: Handbook of Physiology. Principles of feedback control and their application to the respiratory control system. American Physiolological Society, Bethesda, MD, pp 649–680

Dempsey JA, Mitchell GS, Smith CA (1984) Exercise and chemoreception. Am Rev Respir Dis 129:S31–S34

Folgering H (1988) Studying the control of breathing in man. Eur Respir J 1:651–660

Harms C, Dempsey JA (1999) Cardiovascular consequences of exercise hyperpnea. Exerc Sport Sci Rev 27:37–62

Honda Y, Hayashi F, Yoshida A, Ohyabu Y, Nishibayashi Y, Kimura H (1983) Overall "gain" of the respiratory control system in normoxic humans awake and asleep. J Appl Physiol 55:1530–1535

Javaheri S (1999) A mechanism of central sleep apnea in patients with heart failure. N Engl J Med 341:949–954

Khoo MCK (2000) Determinants of ventilatory instability and variability. Respir Physiol 122:167–182

Loeschcke HH (1960) Homoiostase des arteriellen CO_2-drucks und anpassung der lungenventilation an den stoffwechsel als leistungen eines regelsystems. Klin Wochenschr 38:366–376

Milhorn HT Jr (1966) In: The application of control theory to physiological systems. Saunders, Philadelphia, pp 148–157

Mohan R, Duffin J (1997) The effect of hypoxia on the ventilatory response to carbon dioxide in man. Respir Physiol 108:101–115

Ohyabu Y, Yoshida A, Hayashi F, Honda Y (1982) Ventilatory response to CO_2 after brief stimulations of the peripheral chemoreceptors in man. Jpn J Physiol 32:627–636

Oren A, Wasserman K, Davis JA, Whipp BJ (1981) Effect of CO_2 set point on ventilatory response to exercise. J Appl Physiol 51:185–189

Patakas D, Louridas G, Argyropoulou P, Stavropoulos C (1978) Respiratory drive in patients with chronic obstructive pulmonary disease. Respiration 36:194–200

Pianosi P, Grondin D, Desmond K, Coates AL, Aranda JV (1994) Effect of caffeine on the ventilatory response to inhaled carbon dioxide. Respir Physiol 95:311–320

Poon CS, Greene JG (1985) Control of exercise hyperpnea during hypercapnia in humans. J Appl Physiol 59:792–797

Robbins PA (1988) Evidence for interaction between the contributions to ventilation from the central and peripheral chemoreceptors in man. J Physiol 401:503–518

Teppema L, Sarton E, Dahan A, Olievier CN (2000) The neuronal nitric oxide synthase inhibitor 7-nitroindazole (7-NI) and morphine act independently on the control of breathing. Br J Anaesth 84:190–196

Wasserman K, Whipp BJ, Casaburi R (1986) In: Handbook of Physiology. The respiratory system. Control of breathing. American Physiological Society, Bethesda, MD, pp 595–620

Whipp BJ, Pardy RL (1986) In: Handbook of Physiology. Breathing during exercise. American Physiological Society, Bethesda, MD, pp 605–629

Am J Physiol Heart Circ Physiol 287: H2906–H2913, 2004;
doi:10.1152/ajpheart.00035.2004.

A self-calibrating telemetry system for measurement of ventricular pressure-volume relations in conscious, freely moving rats

Kazunori Uemura,[1] Toru Kawada,[1] Masaru Sugimachi,[1] Can Zheng,[1,2,3] Koji Kashihara,[1,3] Takayuki Sato,[4] and Kenji Sunagawa[1]

[1]*Department of Cardiovascular Dynamics, National Cardiovascular Center Research Institute, Suita 565-8565;* [2]*Japan Space Forum, Tokyo 105-0013;* [3]*Organization of Pharmaceutical Safety and Research, Tokyo 100-0013; and* [4]*Department of Cardiovascular Control, Kochi Medical School, Nankoku 783-8505, Japan*

Submitted 15 January 2004; accepted in final form 28 July 2004

Uemura, Kazunori, Toru Kawada, Masaru Sugimachi, Can Zheng, Koji Kashihara, Takayuki Sato, and Kenji Sunagawa. A self-calibrating telemetry system for measurement of ventricular pressure-volume relations in conscious, freely moving rats. *Am J Physiol Heart Circ Physiol* 287: H2906–H2913, 2004; doi:10.1152/ajpheart.00035.2004.—Using Bluetooth wireless technology, we developed an implantable telemetry system for measurement of the left ventricular pressure-volume relation in conscious, freely moving rats. The telemetry system consisted of a pressure-conductance catheter (1.8-Fr) connected to a small (14-g) fully implantable signal transmitter. To make the system fully telemetric, calibrations such as blood resistivity and parallel conductance were also conducted telemetrically. To estimate blood resistivity, we used four electrodes arranged 0.2 mm apart on the pressure-conductance catheter. To estimate parallel conductance, we used a dual-frequency method. We examined the accuracy of calibrations, stroke volume (SV) measurements, and the reproducibility of the telemetry. The blood resistivity estimated telemetrically agreed with that measured using an ex vivo cuvette method ($y = 1.09x - 11.9$, $r^2 = 0.88$, $n = 10$). Parallel conductance estimated by the dual-frequency (2 and 20 kHz) method correlated well with that measured by a conventional saline injection method ($y = 1.59x - 1.77$, $r^2 = 0.87$, $n = 13$). The telemetric SV closely correlated with the flowmetric SV during inferior vena cava occlusions ($y = 0.96x + 7.5$, $r^2 = 0.96$, $n = 4$). In six conscious rats, differences between the repeated telemetries on different days (3 days apart on average) were reasonably small: 13% for end-diastolic volume, 20% for end-systolic volume, 28% for end-diastolic pressure, and 6% for end-systolic pressure. We conclude that the developed telemetry system enables us to estimate the pressure-volume relation with reasonable accuracy and reproducibility in conscious, untethered rats.

conductance catheter; serial reproducibility; volumetric accuracy; dual-frequency method; Bluetooth

SMALL EXPERIMENTAL ANIMALS, such as rats and mice, are widely used in cardiovascular research. These animals can offer a variety of disease models, including heart failure and hypertension, and enable us to analyze the molecular mechanisms of the pathophysiology underlying such diseases (5, 7, 12, 21, 27). To interpret the molecular findings in terms of cardiac phenotype, an accurate assessment of cardiac function, including the contractile properties of the left ventricle (LV), is required. As a load-insensitive index of LV contractility, the end-systolic pressure-volume relation (ESPVR) has been estimated in small animal species with the use of a conductance catheter technique or an ultrasonic crystal method in acute experimental settings (6, 9, 14, 15, 23). However, the anesthesia and thoracotomy required by these techniques inevitably exert adverse effects on the heart (13, 22, 30). In addition, the time course of disease progression or long-term drug effects cannot be assessed in acute experimental settings (7, 16). To overcome these problems, long-term experimental settings should be developed where the LV pressure-volume relation can be measured telemetrically in small experimental animals.

In the present study, we have developed a new telemetry system to measure LV volume, pressure, and electrocardiogram (ECG) in conscious, freely moving rats. In this system, the LV pressure-volume relation was obtained from a pressure-conductance catheter chronically implanted in the rat LV. To calibrate the conductance signal and obtain absolute LV volume, measurements of blood resistivity (ρ) and parallel conductance (G_p) are required (3, 4). These calibration procedures require blood sampling and hypertonic saline infusion, but such ex vivo procedures are not applicable to conscious, freely moving small animals. To circumvent such ex vivo procedures in our new telemetry system (29), we adopted a self-calibrating method for the LV volume measurement, as reported in our previous study (28). The aim of the present study was therefore to develop a telemetry system and evaluate its performance. Our results indicate that we succeeded in measuring the LV pressure-volume relation in conscious, untethered rats with reasonable accuracy and reproducibility.

METHODS

Implantable Pressure-Volume Telemetry System

Figure 1*A* illustrates a newly developed pressure-volume telemetry system for rats; it consists of a pressure-conductance catheter, an analog processor-transmitter (weight = 14 g, volume = 11 ml), and a battery unit (lithium battery; weight = 12 g, volume = 10 ml).

Pressure-conductance catheter. Details of the pressure-conductance catheter are presented in Fig. 1*B*. To measure LV conductance, four platinum electrodes (0.25 mm wide) were used. Constant excitation current was applied to the two outermost electrodes while the voltage signal associated with LV conductance was measured from the two inner sensing electrodes. To measure LV pressure, a high-fidelity pressure transducer (Millar Instruments, Houston, TX) was mounted between the two sensing electrodes for the LV conductance measurement. To measure ρ, four smaller platinum electrodes (0.1 mm wide, 0.2 mm between centers of adjacent electrodes, 0.6 mm

Address for reprint requests and other correspondence: K. Uemura, Dept. of Cardiovascular Dynamics, National Cardiovascular Center Research Institute, 5-7-1, Fujishirodai, Suita 565-8565, Japan (E-mail: kuemura@ri.ncvc.go.jp).

The costs of publication of this article were defrayed in part by the payment of page charges. The article must therefore be hereby marked "*advertisement*" in accordance with 18 U.S.C. Section 1734 solely to indicate this fact.

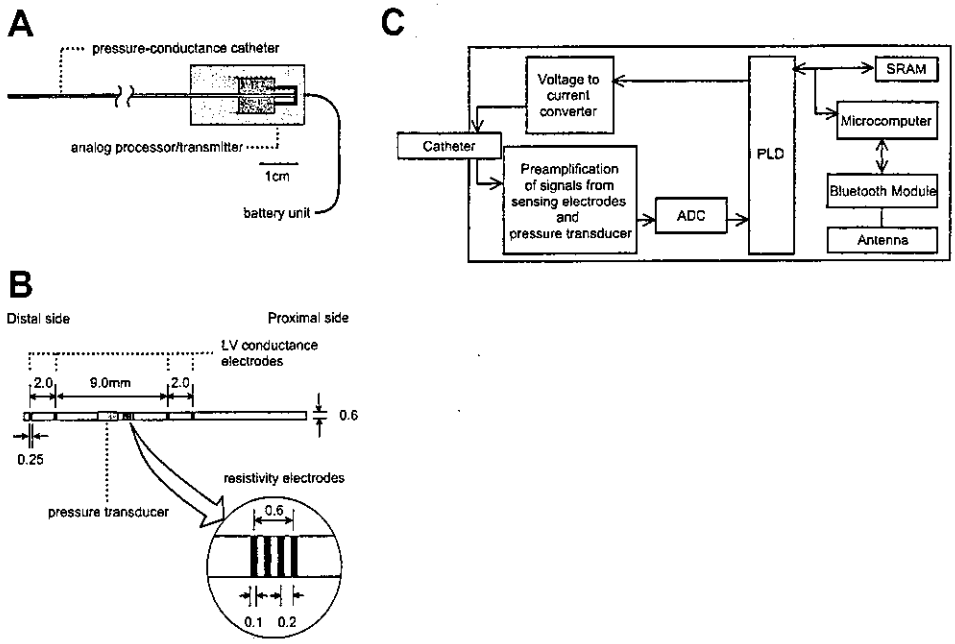

Fig. 1. *A*: schematic illustration of our pressure-volume telemetry system. A 10-cm-long pressure-conductance catheter obtains signals of left ventricular (LV) conductance and pressure, intraventricular blood resistivity, and an ECG. Signals are processed and transmitted by an analog processor transmitter, which is powered by a battery unit (lithium battery). *B*: schematic illustration of our pressure-conductance catheter. Catheter has 4 electrodes for measurement of LV conductance and 4 electrodes for measurement of intraventricular blood resistivity (*inset*). A high-fidelity pressure transducer is mounted between *electrodes 2* and *3*. *C*: block diagram of an analog processor transmitter. ADC, analog-to-digital converter; PLD, programmable logic device; SRAM, static random access memory.

between centers of excitation electrodes) were placed near the pressure transducer (Fig. 1*B*, *inset*). Constant excitation current was applied to the two outer electrodes while the voltage signal associated with ρ was measured from the two inner electrodes.

Analog processor transmitter. A block diagram of the analog processor transmitter is presented in Fig. 1*C*. It was equipped with several functions. First, it delivered a dual-frequency (2 and 20 kHz) constant excitation current [20 μA root mean square (RMS)] for measurements of LV conductance and ρ. We validated the current output by injecting it into known resistors and examining the developed voltage. The resulting RMS current output was 20.4 μA (SD 0.2) and 19.3 μA (SD 0.2) at 2 and 20 kHz, respectively. These values were constant over different resistors (50–990 Ω). Second, it measured and processed the voltage signal from the sensing electrodes as follows: Analog signals were digitized (12 bits, 40-kHz sampling rate; model ADS7870, Texas Instruments, Dallas, TX) and then fed into a programmable logic device (model XC 2C256, Xilinx, San Jose, CA), which processed them to yield RMS digital signals corresponding to frequency components of 2 and 20 kHz and a low-frequency signal (<2 kHz; see APPENDIX). The circuit was connected to the larger or smaller electrodes in response to a command signal, so that LV conductance or ρ could be measured. Third, the analog processor-transmitter had a bridge amplifier for the LV pressure measurement. The LV pressure signal was also digitized (12 bits, 40-kHz sampling rate). All these functions were controlled by a microcomputer (model H8S, Hitachi, Tokyo, Japan).

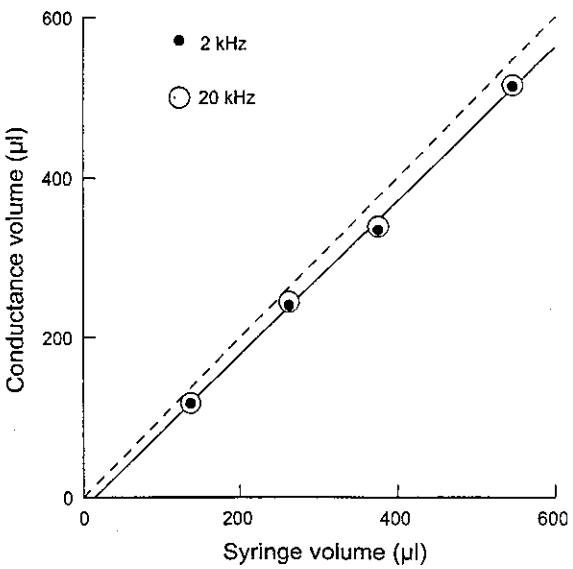

Fig. 2. Comparison of conductance-derived volumes at 2 and 20 kHz vs. known fluid volumes of syringes. Both conductance-derived volumes were essentially identical for each of the syringe volumes. Relation between conductance-derived volume and syringe volume was quite linear. Solid line, regression between conductance-derived volume at 20 kHz and syringe volume; dashed line, identity.

Bluetooth technology was used to transmit the data (18). For real-time monitoring, all processed signals were resampled at 200 Hz by the microcomputer and transmitted to an external receiver (CASIRA, CSR, Cambridge, UK) by a Bluetooth module (model LMBTB027, Murata, Tokyo, Japan). For high-precision non-real-time analysis, signals recorded at 2,000 Hz over a 6-s interval were stored in a static random access memory (model HM62V16256, Hitachi) and then transmitted to the receiver by the Bluetooth module. The external receiver detected the radio-frequency signal from the transmitter and converted it to a serial bit stream.

Self-Calibration of Ventricular Volumetry

The principles of conductance volumetry have been described previously (3, 4). Briefly, the ventricular conductance signal (G) can be converted to absolute ventricular volume (V) as follows

$$V = (1/\alpha)\,(L^2 \cdot \rho)\,(G - G_p) \qquad (1)$$

where α is a volume calibration factor, L is the distance between the sensing electrodes, ρ is blood resistivity, and G_p is parallel conductance. L was 9 mm in the present catheter design.

In a preliminary experiment, when the catheter was placed in a series of graduated syringes filled with diluted saline, conductance-derived volumes at 2 and 20 kHz were close to the true syringe volume in the volume range of interest (Fig. 2). Conductance-derived volumes at the two frequencies were essentially identical for each of the syringe volumes. Hence, α was assumed to be unity in the present study (14, 23).

The four smaller electrodes were used to estimate ρ (Fig. 1*B*, *inset*). The distance between the excitation electrodes was set at 0.6 mm. In an in vitro experiment, we confirmed that the current distribution volume was confined to an ~4-mm diameter around the catheter with this electrode design (see APPENDIX). The end-diastolic LV diameter is 7–9 mm in normal rats and 9–12 mm in rats with left heart failure (17). Because the interelectrode distance between the excitation electrodes was small enough to confine the current distribution volume to within the end-diastolic ventricular blood pool in the rat LV, we estimated ρ at end diastole (10, 28).

G_p was estimated by the dual-frequency excitation method (8, 9, 28) as follows

$$G_p = \kappa \times \Delta G_{20-2} \quad (2)$$

where ΔG_{20-2} is the difference in ventricular conductance values between the 20- and 2-kHz excitation frequencies and κ is an experimentally derived constant. Once κ is determined, G_p can be estimated from ΔG_{20-2}, obviating the need for saline infusion.

Instrumentation and Experimental Protocols

Thirty-three male Sprague-Dawley rats (350–400 g body wt) were used. Care of the animals was in strict accordance with the *Guiding Principles for the Care and Use of Animals in the Field of Physiological Sciences* as approved by the Physiological Society of Japan. The animals were anesthetized with pentobarbital sodium (50 mg/kg ip) and ventilated artificially. A vertical midline cervical incision was made to expose the right common carotid artery while the animal was in the supine position. The pressure-conductance catheter of the telemetry system was inserted into the LV retrogradely from the right common carotid artery. The position of the catheter was verified by monitoring the pressure-volume signal and by two-dimensional echocardiography. At the conclusion of the experiment, the animal was killed with an overdose of pentobarbital sodium, and the heart was examined to reconfirm the proper positioning of the catheter.

Group 1 (n = 23). We evaluated the accuracy of telemetric calibration of ρ and G_p under anesthetized, closed-chest conditions. Catheters (3-Fr) were inserted into the right and left jugular veins for blood sampling and saline injection, respectively. In 10 of the 23 rats, we compared ρ estimated telemetrically (ρ_{est}) with ρ measured from sampled blood by a conventional ex vivo cuvette method (ρ_{conv}). In the remaining 13 rats, we estimated G_p by the dual-frequency excitation method ($G_{p,est}$) and by the hypertonic saline method ($G_{p,conv}$). To obtain $G_{p,conv}$, we injected 20 μl of saturated saline into the right jugular vein while continuously measuring LV conductance (14, 23). To obtain $G_{p,est}$, we measured LV conductance at 2- and 20-kHz excitation frequencies and derived ΔG_{20-2} by averaging the instantaneous conductance difference over ~10 cardiac cycles. We randomly selected 7 of the 13 rats and determined the proportionality constant (κ in *Eq. 2*) from the averaged ratio of $G_{p,conv}$ to ΔG_{20-2}. $G_{p,est}$ and $G_{p,conv}$ were measured while the artificial ventilation was temporarily suspended at end expiration.

Group 2 (n = 4). Under anesthetized, open-chest conditions, we evaluated the accuracy of volumetry by comparing stroke volume (SV) measured by the telemetry system with SV measured by an ultrasonic flowmeter (model 2.5S273, Transonic Systems, Ithaca, NY). After median sternotomy, the aortic arch was dissected free from surrounding tissues. A flow probe was placed around the ascending aorta to measure the aortic blood flow. A string occluder was placed loosely around the inferior vena cava to decrease the LV preload and vary the SV over a wide range. We simultaneously measured the telemetric LV volume and the ultrasonic aortic blood flow while varying the preload. The measurements were done while the artificial ventilation was temporarily suspended at end expiration.

Group 3 (n = 6). Under conscious, closed-chest conditions, we evaluated the reproducibility of the telemetry on different days. Aseptic conditions were maintained throughout the surgical procedure. The telemetry system was implanted in a subcutaneous pocket made at the right upper dorsum. The skin was closed, and the animal was allowed to recover from anesthesia. On the day after implantation surgery, the LV volume, pressure, and an ECG were measured telemetrically in the fully recovered, conscious animal (*study 1*). Each rat underwent a second set of telemetric measurements at 1–6 days after the initial study (*study 2*). Ambient barometric pressure was measured simultaneously and subtracted from the telemetric LV pressure to compensate for changes in atmospheric pressure.

Data Collection

We used the real-time mode (200-Hz sampling) of the telemetry system and recorded LV conductance, LV pressure, intraventricular ECG, and ρ on a hard disk of a dedicated laboratory computer system (model HFPA031003, Epson, Tokyo, Japan). In *group 2*, ultrasonic aortic blood flow was digitized at 1,000 Hz through a 12-bit analog-to-digital converter and stored on a hard disk for subsequent analyses.

Statistical Analysis

For the calculation of LV volume using *Eq. 1*, *G* and ρ were obtained from the 20-kHz frequency component. In *group 1*, we used linear regression analysis to compare the telemetric and conventional measurements of ρ (ρ_{est} vs. ρ_{conv}) and G_p ($G_{p,est}$ vs. $G_{p,conv}$). In *group 2*, we calculated the telemetric SV from the difference between the end-diastolic volume (EDV) and end-systolic volume (ESV) in each beat. The flowmetric SV was computed from the time integral of aortic blood flow. The telemetric SV was compared with the flowmetric SV by linear regression analysis. In *group 3*, we compared heart rate (HR), EDV, ESV, end-diastolic pressure (EDP), and end-systolic pressure (ESP) between *study 1* and *study 2* for each rat. Using the pressure-volume data, we calculated ejection fraction (EF), maximal pressure increase ($+dP/dt_{max}$) or decrease ($-dP/dt_{max}$) over time, and the time constant of isovolumic relaxation (τ) and compared them between *study 1* and *study 2* for each rat. A nonparametric multiple comparison (Wilcoxon's signed-rank test) was used to examine the difference in each parameter between *study 1* and *study 2*. Group data are expressed as means (SD). Differences were considered significant at $P < 0.05$.

RESULTS

Telemetric Calibration of ρ

Figure 3*A* is a representative time series showing LV pressure and ρ at 2 and 20 kHz derived from the telemetry. The bottom of the ρ waveform, which corresponded to end diastole, represents the time when there was sufficient blood volume around the catheter (10). The lowest ρ values at 2 kHz ($\rho_{2\,kHz}$) and 20 kHz ($\rho_{20\,kHz}$) were very close (197 and 207 Ω·cm, respectively). This was the case for all the rats, indicating that ρ was frequency independent ($\rho_{2\,kHz} = 1.08\rho_{20\,kHz} - 13.8$, $r^2 = 0.96$, SE of the estimate = 6.7 Ω·cm) (6, 9). The lowest ρ at 20 kHz was treated as ρ_{est}.

Figure 3*B* summarizes the relation between ρ_{est} and ρ_{conv} obtained from 10 rats in *group 1*. ρ_{est} agreed with ρ_{conv} reasonably well ($\rho_{est} = 1.09\rho_{conv} - 11.9$, $r^2 = 0.88$, SE of the estimate = 10.7 Ω·cm). The ratio of SE of the estimate to the mean of ρ_{est} was 0.046, indicating small variability around the regression line.

Telemetric Calibration of G_p

Figure 4*A* illustrates a representative time series of telemetrically measured ECG, LV conductance signals at 2 and 20 kHz, and LV pressure. In this animal, ΔG_{20-2} was 0.56 mS

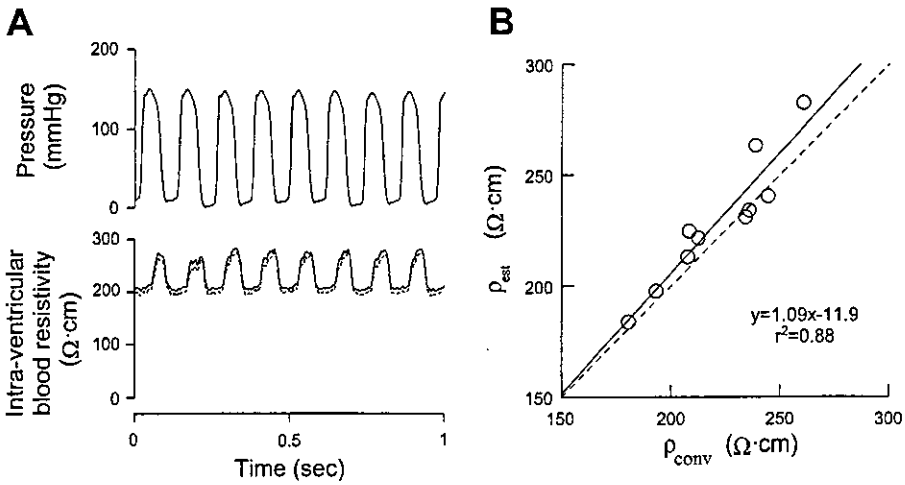

Fig. 3. *A*: waveforms of ventricular pressure and intraventricular blood resistivity at 2 kHz (dashed line) and 20 kHz (solid line) as a function of time obtained telemetrically. *B*: relation between blood resistivity as measured in a cuvette (ρ_{conv}) and as estimated via catheter electrodes (ρ_{est}) in 10 rats. Solid line, regression; dashed line, identity.

and $G_{p,conv}$ was 3.27 mS. Therefore, κ was calculated to be 5.79 from *Eq. 2* in this animal. The averaged κ from seven randomly selected rats was 5.14, which we used as the experimentally derived constant to obtain $G_{p,est}$ for all rats.

Figure 4*B* summarizes the relation between $G_{p,est}$ and $G_{p,conv}$ obtained from 13 rats in *group 1*. $G_{p,est}$ correlated well with $G_{p,conv}$ ($G_{p,est} = 1.59G_{p,conv} - 1.77$, $r^2 = 0.87$, SE of the estimate = 0.33 mS). The ratio of SE of the estimate to the mean of $G_{p,est}$ was 0.11, indicating that the estimation was reasonable around the mean of $G_{p,est}$.

Accuracy of the Televolumetry

Figure 5*A* depicts LV pressure and volume measured by telemetry and aortic blood flow measured by the ultrasonic flowmeter. Vena caval occlusion decreased LV pressure, volume, and aortic blood flow.

Figure 5*B* summarizes the relation between telemetric SV (SV_{tele}) and flowmetric SV (SV_{flow}) obtained from four rats in *group 2*. SV_{tele} matched SV_{flow} reasonably well in each of the four rats: $r^2 = 0.90-0.99$, slope = 0.86 (SD 0.16), intercept = 12.4 μl (SD 10.4), and SE of the estimate = 4.3 μl (SD 0.4). A linear regression analysis on the pooled data from all four rats also showed a highly linear relation between SV_{tele} and SV_{flow}: $SV_{tele} = 0.96SV_{flow} + 7.5$, $r^2 = 0.96$, SE of the estimate = 6.6 μl. The ratio of SE of the estimate to the mean of SV_{tele} was 0.10.

Reproducibility of the Telemetry

Individual data obtained by the telemetry system for all six rats in *group 3* are provided in Tables 1 and 2. The overall variability between repeated measurements in the same rat was reasonably small. There were no significant differences in repeated measurements of HR, EDV, ESV, EDP, and ESP between *study 1* and *study 2* (Table 1). There were no significant differences in repeated measurements of EF, $+dP/dt_{max}$, $-dP/dt_{max}$, and τ between *study 1* and *study 2* (Table 2).

Figure 6 illustrates the representative LV pressure-volume loops obtained from a rat in *group 3*. The pressure-volume loops in *studies 1* and *2* were almost identical.

DISCUSSION

We have developed a novel telemetry system for measurements of LV volume, pressure, and ECG in conscious, freely moving rats. The system, for the first time to the best of our knowledge, has enabled measurement of the LV pressure-

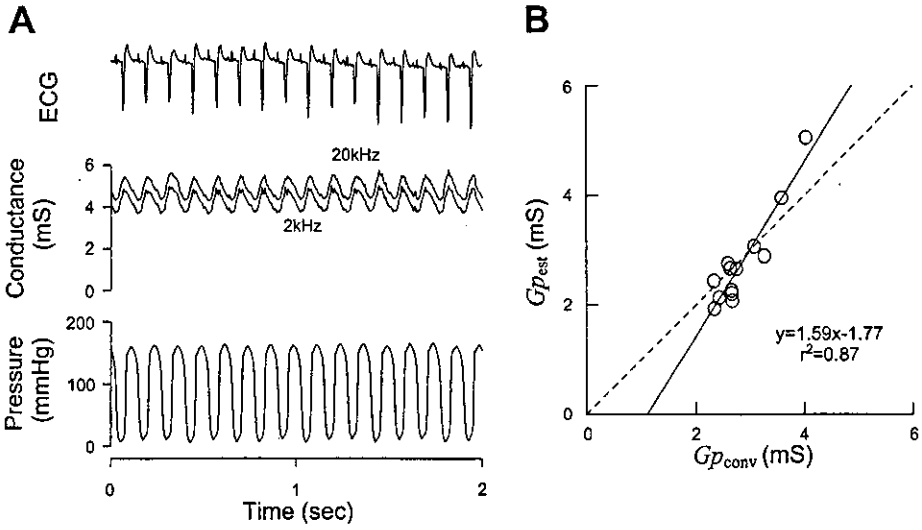

Fig. 4. *A*: waveforms of an ECG, conductance signals at 2 and 20 kHz, and ventricular pressure as a function of time, obtained telemetrically. *B*: relation between parallel conductance estimated by the saline infusion method ($G_{p,conv}$) and by dual-frequency excitation method ($G_{p,est}$) in 13 rats. Solid line, regression; dashed line, identity.

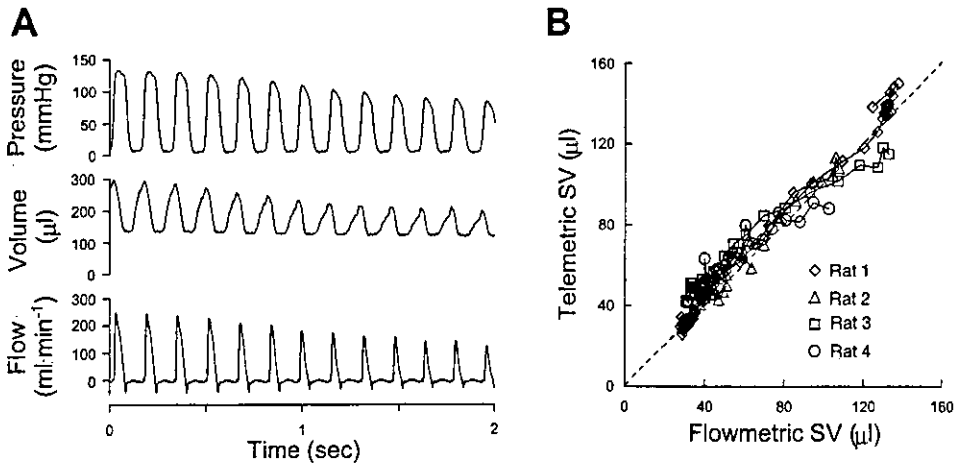

Fig. 5. *A*: representative traces of ventricular pressure, ventricular volume obtained telemetrically, and aortic flow measured by an ultrasonic flowmeter during vena cava occlusion in 1 rat. *B*: relation between telemetric stroke volume (SV) and flowmetric SV in 4 rats. Dashed line, identity.

volume relation in small experimental animals, such as rats, under completely conscious, unrestricted conditions with reasonably good accuracy and reproducibility.

Self-Calibrating Volumetry

In our conductance volumetric system, ρ and G_p were estimated using the telemetric signals alone (Figs. 3 and 4). We will be able to use the empirical constant κ (=5.14), determined in this study, in the future application of our telemetry system to rats. The self-calibrating feature made it possible to measure the LV pressure-volume relation in rats without tethering them for ex vivo calibration procedures, such as blood sampling and hypertonic saline infusion. Besides their impracticality in conscious, small animals, these procedures can alter hemodynamic conditions (6, 9). Frequent blood sampling can induce anemia. Concentrated saline injection depresses myocardial contractility and has volume-loading effects (6, 9). Our telemetry system is free of these problems.

The current used for resistivity measurements was distributed in a 2-mm radius around the catheter (see APPENDIX). The ratio of the radius (i.e., penetration depth) to the distance between the excitation electrodes was ~3 (≒2/0.6). This ratio is at odds with previously reported values, which were around or less than unity (6, 10, 26). Penetration depth is affected by the relation between the resistivity of the target tissue and that of the surrounding structure (26). This relation in our study was different from those in previous studies, which would be one reason for the discrepancy. Difference in shape and arrangement of the electrodes between our system and those previous studies would be another reason. Because the electrodes were placed very closely, stray capacitance between connecting wires could be a problem (31). The fact that resistivity values at 2 and 20 kHz were very close indicated that our titration method effectively removed the problem of stray capacitance (see APPENDIX). However, it might be better to incorporate techniques such as capacitance neutralization to completely prevent the problem, in case the capacitance were to significantly affect our titration accuracy in future long-term use, e.g., with increases in electrode impedance (31).

We used the dual-frequency excitation method previously described by Gawne et al. (8). Feldman et al. (6) combined measured resistivity of the myocardium with an analytic approach and estimated G_p from the conductance signals at 10 and 100 kHz. Although their method was completely independent of saline injection, it required measurement of myocardial resistivity with an additional four-electrode sensor.

Volumetric Accuracy and Reproducibility

We have verified the volumetric accuracy of our telemetry system by comparing SV_{tele} with SV_{flow} during inferior vena cava occlusions (Fig. 5*A*). The volumetric accuracy of the conductance catheter technique in the rat heart has been ex-

Table 1. *Reproducibility of hemodynamic variables*

	HR, beats/min		EDV, μl		ESV, μl		EDP, mmHg		ESP, mmHg	
Rat	S1	S2	S1	S2	S1	S2	S1	S2	S1	S2
1	530	475	303	307	168	182	14	19	131	123
2	363	476	310	280	212	151	11	17	121	133
3	426	500	330	355	212	220	12	9	127	129
4	405	511	244	194	143	89	14	13	120	125
5	402	382	364	434	269	326	15	14	119	106
6	400	380	240	283	158	167	24	36	142	152
Mean (SD)	421 (57.3)	454 (58.2)	299 (49)	309 (81)	194 (47)	189 (80)	15 (5)	18 (10)	127 (9)	128 (15)
Difference										
Mean (SD)	65 (40)		37 (23)		34 (26)		5 (4)		8 (4)	
Percent difference										
Mean (SD)	15 (9)		13 (8)		20 (17)		28 (16)		6 (4)	

S1, *study 1;* S2, *study 2;* HR, heart rate; EDV, left ventricular end-diastolic volume; ESV, left ventricular end-systolic volume; EDP, left ventricular end-diastolic pressure; ESP, left ventricular end-systolic pressure.

Table 2. *Reproducibility of parameters of ventricular functions*

Rat	EF, %		+dP/dt$_{max}$, mmHg/s		−dP/dt$_{max}$, mmHg/s		τ, ms	
	S1	S2	S1	S2	S1	S2	S1	S2
1	45	41	10,594	9,615	7,165	6,648	9.2	9.0
2	32	46	9,284	11,802	6,364	7,372	8.5	8.3
3	36	38	10,373	12,129	7,277	6,937	9.4	8.1
4	42	54	9,274	11,801	7,527	7,013	6.4	9.5
5	26	25	8,862	7,610	6,132	4,878	7.4	7.9
6	34	41	9,808	9,756	7,518	7,273	11.0	12.4
Mean (SD)	36 (7)	41 (10)	9,699 (682)	10,452 (1,773)	6,997 (601)	6,687 (923)	8.7 (1.6)	9.2 (1.7)
Difference								
Mean (SD)	7 (5)		1513 (957)		646 (397)		1.1 (1.1)	
Percent difference								
Mean (SD)	17 (13)		15 (9)		10 (7)		13 (14)	

EF, left ventricular ejection fraction; dP/dt$_{max}$, maximal pressure rise (+) or decrease (−) over time; τ, time constant of isovolumic left ventricular relaxation.

amined using a similar comparison (14, 23). Ito et al. (14) reported a very high and linear correlation (r = 0.97–0.99) between conductance-derived SV and SV measured by an electromagnetic flowmeter in rats. We also obtained a similar highly linear relation between SV_{tele} and SV_{flow} (Fig. 5*B*).

The reproducibility of our telemetry system (Table 1) is good enough for many applications, such as the study of LV remodeling in rats. This is because EDV has been reported to increase to ~200% of the control value in rats with ischemic heart failure and in heart failure-prone rats (2, 7, 12).

Applications of the Telemetry System

The developed telemetry system enables detailed evaluation of cardiac function in small animals by eliminating the effects of anesthesia and acute surgical intervention (13, 22, 30). By using a single-beat estimation method to determine the ESPVR, our system would enable evaluation of the load-independent contractile index in conscious animals (24, 25). We validated pressure-volume signals only under control conditions in this study. The stability of the acquired data and the capacity of our system to monitor altered hemodynamics remain to be evaluated.

Our telemetry system is potentially useful for the long-term monitoring of LV function. We confirmed that our system was viable for up to 8 days in this study. However, further studies are required to definitively evaluate the longevity of the implants over a longer period of time (19). Thrombosis and infection would affect the morbidity and mortality associated with the chronic implantation of our system. Coating of the pressure-conductance catheter with anticoagulants and further miniaturization of the implant are under development to ameliorate such problems.

We adopted Bluetooth technology for telecommunication. Bluetooth is a wireless technology designed to allow low-cost, short-range radio links between mobile personal computers and other portable devices (18). While point-to-point connections are supported, Bluetooth technology allows up to seven simultaneous connections to be established and maintained by a single receiver (18). This unique feature of Bluetooth technology should be beneficial in experimental settings where a large population of animals in a single cage must be evaluated (16).

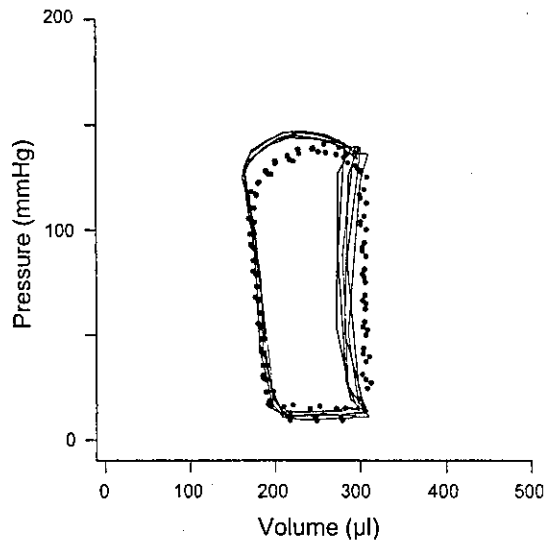

Fig. 6. Day-to-day reproducibility of LV pressure-volume loops in 1 rat. Thick solid loops, *study 1*; dotted loops, *study 2*. Loops for *studies 1* and *2* (6 days apart) were superimposable.

Limitations

The volume calibration factor α was assumed to be unity on the basis of the preliminary experiment, where the conductance-derived volume was close to true syringe volume in the normal operating range for rats (Fig. 2). Georgakopoulos and Kass (9) noted that the relation was quite linear when the volume range was limited to the physiological operating range for mice. Hettrick et al. (11) also noted that conductance-derived volume was close to true syringe volume and α was unity in a volume range. However, both groups and others noted that the relation was nonlinear when considered over a wider volume range (1, 9, 11, 20). In addition, the syringes have no G_p, whereas the rat heart does. It has been shown that G_p has significant effects on α (11). Taken together, these findings suggest that it will be necessary to recalibrate α when we apply our system to the rat LV in heart failure or other cardiac disorders, where drastic changes in ventricular volume and changes in the electrical properties of surrounding structures, i.e., change in G_p, are probable (1).

Values of EF in Table 2 are low for normal rats (5, 7). Other parameters of LV function are, however, within the normal

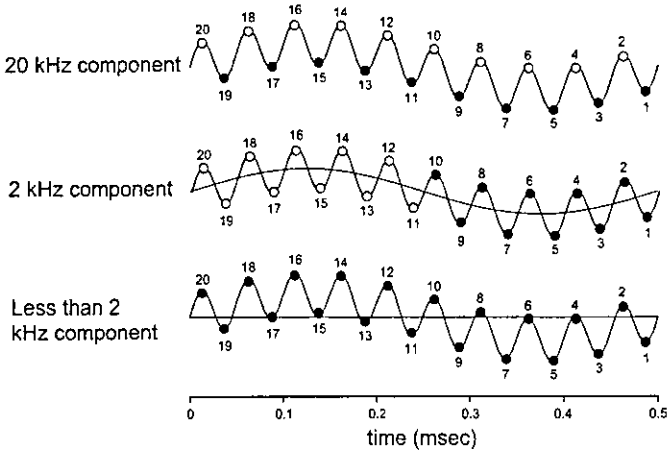

Fig. 7. Visual representation of logical processing used to extract 20-, 2-, and <2-kHz frequency components of digital signals.

range (5, 7) (Table 2). Dual-frequency derived G_p values from the rats in *group 3* ranged from 1.8 to 3.3 mS (mean 2.3 ± 0.4 mS). The dual-frequency method slightly underestimated G_p in that range compared with the saline injection method (Fig. 4*B*). This might result in an apparent reduction of EF. To settle the discrepancy between EF and other functional parameters, it is necessary to compare the telemetric EF with the EF determined by other independent methods, such as echocardiography.

We were able to estimate ρ in the LV cavity in normal-sized rats with the present catheter design (Fig. 1*B*, *inset*). However, the catheter design may not be applicable to smaller rats or mice, where the current distribution volume probably distributes outside the LV cavity. To apply our system to these small animals, further reduction of the interelectrode distance is required for measurement of ρ.

Conclusion

A novel telemetry system was developed for measurements of LV pressure, volume, and ECG in conscious, freely moving rats. The system enabled us to accurately measure the LV pressure-volume relation with good reproducibility and without the harmful effects of anesthesia or acute surgical trauma in rats.

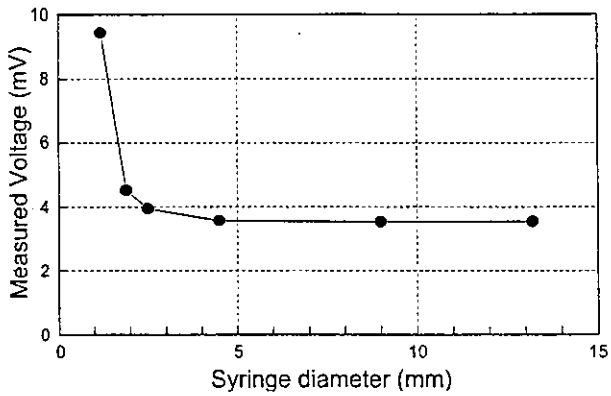

Fig. 8. Relation between syringe diameter and voltage as measured by sensing electrodes of our conductance catheter designed for blood resistivity measurement. Voltage reaches a minimum at a syringe diameter of ~4 mm. This indicates that current distribution volume is confined to within a 4-mm diameter around the catheter.

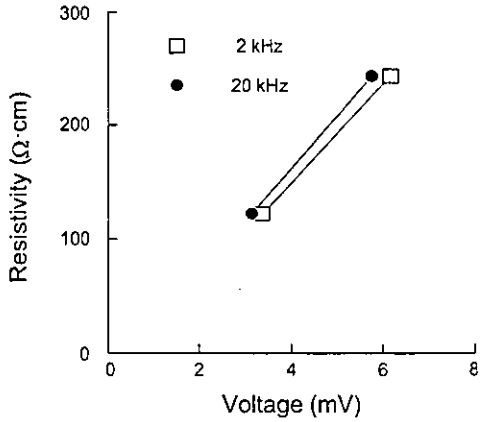

Fig. 9. Relation between measured voltage and saline resistivity.

APPENDIX

Logical processing of digital signals to extract frequency components. We extracted frequency components of 20 kHz, 2 kHz, and low frequency (<2 kHz) by logical processing of digital signals. The analog signals were converted to digital signals at a sampling rate of 40 kHz. Twenty serial digital values were processed simultaneously (Fig. 7). We obtained the 20-kHz component on the basis of the difference between even- and odd-numbered digital values. We calculated an average of every 10 digital values. We obtained the 2-kHz component on the basis of the difference between the two averaged values of the former half and the latter half (average of 10 values each). We obtained the low-frequency component by averaging all 20 digital values. All this logical processing was performed by the programmable logic device (Fig. 1*C*).

Estimation of intraventricular ρ. First, we experimentally determined the current distribution volume of the four small electrodes for estimation of ρ. We placed our pressure-conductance catheter at the center of plastic syringes of various sizes filled with diluted saline. Saline resistivity was matched to that of the blood (122 Ω·cm). We injected a constant current (20 kHz, 20 μA RMS) into the excitation electrodes (0.6 mm apart; Fig. 1*B*, *inset*) and measured voltage via the sensing electrodes. We present the relation between the measured voltage and the syringe diameter in Fig. 8. As demonstrated, with increasing syringe diameter, the voltage signal decreased and reached a minimum at a syringe diameter of ~4 mm. This implied that most (>95%) of the current was confined to within the cylindrical diameter at which the voltage reached a minimum. From these data, we concluded that the current distribution volume was confined to within a 4-mm diameter around the catheter.

Second, the resultant voltage signal was converted to ρ by a conversion formula. We determined the conversion formula experimentally by placing the catheter at the center of a plastic syringe with a diameter of 9 mm. Syringes were filled with diluted saline solutions with known resistivities in the range of those expected in rat blood (122 and 244 Ω·cm). Constant currents (20 and 2 kHz, 20 μA RMS) were injected between the excitation electrodes. We linearly related the measured RMS voltage to saline resistivity and used this relation as a conversion formula (Fig. 9).

ACKNOWLEDGMENTS

This study was presented in part at the Scientific Sessions of the American Heart Association, Orlando, FL, November 2003.

GRANTS

This study was supported by Ministry of Health Labour and Welfare of Japan Health and Labour Sciences Research Grants for Research on Advanced Medical Technology 13090401 and H14-Nano-002 and Japan Society for the Promotion of Science Grants-in-Aid for Scientific Research A 15200040, C

14570707, and C 15590786, by a Ground-Based Research Grant for space utilization promoted by the National Space Development Agency of Japan and the Japan Space Forum, and by the Program for Promotion of Fundamental Studies in Health Science of the Organization for Pharmaceutical Safety and Research of Japan.

REFERENCES

1. **Applegate RJ, Cheng CP, and Little WC.** Simultaneous conductance catheter and dimension assessment of left ventricle volume in the intact animal. *Circulation* 81: 638–648, 1990.
2. **Asanoi H, Ishizaka S, Kameyama T, Nozawa T, Miyagi K, and Sasayama S.** Serial reproducibility of conductance catheter volumetry of left ventricle in conscious dogs. *Am J Physiol Heart Circ Physiol* 262: H911–H915, 1992.
3. **Baan J, Jong TT, Kerkhof PL, Moene RJ, van Dijk AD, van der Velde ET, and Koops J.** Continuous stroke volume and cardiac output from intra-ventricular dimensions obtained with impedance catheter. *Cardiovasc Res* 15: 328–334, 1981.
4. **Baan J, van der Velde ET, de Bruin HG, Smeenk GJ, Koops J, van Dijk AD, Temmerman D, Senden J, and Buis B.** Continuous measurement of left ventricular volume in animals and humans by conductance catheter. *Circulation* 70: 812–823, 1984.
5. **Cingolani OH, Yang XP, Cavasin MA, and Carretero OA.** Increased systolic performance with diastolic dysfunction in adult spontaneously hypertensive rats. *Hypertension* 41: 249–254, 2003.
6. **Feldman MD, Mao Y, Valvano JW, Pearce JA, and Freeman GL.** Development of a multifrequency conductance catheter-based system to determine LV function in mice. *Am J Physiol Heart Circ Physiol* 279: H1411–H1420, 2000.
7. **Francis J, Weiss RM, Wei SG, Johnson AK, and Felder RB.** Progression of heart failure after myocardial infarction in the rat. *Am J Physiol Regul Integr Comp Physiol* 281: R1734–R1745, 2001.
8. **Gawne TJ, Gray KS, and Goldstein RE.** Estimating left ventricular offset volume using dual-frequency conductance catheters. *J Appl Physiol* 63: 872–876, 1987.
9. **Georgakopoulos D and Kass DA.** Estimation of parallel conductance by dual-frequency conductance catheter in mice. *Am J Physiol Heart Circ Physiol* 279: H443–H450, 2000.
10. **Gopakumaran B, Osborn P, Petre JH, and Murray PA.** A new technique to measure and track blood resistivity in intracardiac impedance volumetry. *J Clin Monit* 13: 363–371, 1997.
11. **Hettrick DA, Battocletti JH, Ackmann JJ, Linehan JH, and Warltier DC.** Effects of physical parameters on the cylindrical model for volume measurement by conductance. *Ann Biomed Eng* 25: 126–134, 1997.
12. **Heyen JR, Blasi ER, Nikula K, Rocha R, Daust HA, Frierdich G, Van Vleet JF, De Ciechi P, McMahon EG, and Rudolph AE.** Structural, functional, and molecular characterization of the SHHF model of heart failure. *Am J Physiol Heart Circ Physiol* 283: H1775–H1784, 2002.
13. **Hoit BD, Ball N, and Walsh RA.** Invasive hemodynamics and force-frequency relationships in open- versus closed-chest mice. *Am J Physiol Heart Circ Physiol* 273: H2528–H2533, 1997.
14. **Ito H, Takaki M, Yamaguchi H, Tachibana H, and Suga H.** Left ventricular volumetric conductance catheter for rats. *Am J Physiol Heart Circ Physiol* 270: H1509–H1514, 1996.
15. **Kubota T, Mahler CM, McTiernan CF, Wu CC, Feldman MD, and Feldman AM.** End-systolic pressure-dimension relationship of in situ mouse left ventricle. *J Mol Cell Cardiol* 30: 357–363, 1998.
16. **Lapointe N, Blais C Jr, Adam A, Parker T, Sirois MG, Gosselin H, Clement R, and Rouleau JL.** Comparison of the effects of an angiotensin-converting enzyme inhibitor and a vasopeptidase inhibitor after myocardial infarction in the rat. *J Am Coll Cardiol* 39: 1692–1698, 2002.
17. **Litwin SE, Katz SE, Morgan JP, and Douglas PS.** Serial echocardiographic assessment of left ventricular geometry and function after large myocardial infarction in the rat. *Circulation* 89: 345–354, 1994.
18. **Lou E, Fedorak MV, Hill DL, Raso JV, Moreau MJ, and Mahood JK.** Bluetooth wireless database for scoliosis clinics. *Med Biol Eng Comput* 41: 346–349, 2003.
19. **Mills PA, Huetteman DA, Brockway BP, Zwiers LM, Gelsema AJ, Schwartz RS, and Kramer K.** A new method for measurement of blood pressure, heart rate, and activity in the mouse by radiotelemetry. *J Appl Physiol* 88: 1537–1544, 2000.
20. **Mur G and Baan J.** Computation of the input impedances of a catheter for cardiac volumetry. *IEEE Trans Biomed Eng* 31: 448–453, 1984.
21. **Murphy AM, Kogler H, Georgakopoulos D, McDonough JL, Kass DA, Van Eyk JE, and Marban E.** Transgenic mouse model of stunned myocardium. *Science* 287: 488–491, 2000.
22. **Price HL and Ohnishi ST.** Effects of anesthetics on the heart. *Fed Proc* 39: 1575–1579, 1980.
23. **Sato T, Shishido T, Kawada T, Miyano H, Miyashita H, Inagaki M, Sugimachi M, and Sunagawa K.** ESPVR of in situ rat left ventricle shows contractility-dependent curvilinearity. *Am J Physiol Heart Circ Physiol* 274: H1429–H1434, 1998.
24. **Sato T, Shishido T, Miyashita H, Yoshimura R, and Sunagawa K.** Single-beat estimation of end-systolic elastance (E_{es}) in rats (Abstract). *Circulation* 96 *Suppl* I: I-518, 1997.
25. **Shishido T, Hayashi K, Shigemi K, Sato T, Sugimachi M, and Sunagawa K.** Single-beat estimation of end-systolic elastance using bilinearly approximated time-varying elastance curve. *Circulation* 102: 1983–1989, 2000.
26. **Steendijk P, Mur G, Van Der Velde ET, and Baan J.** The four-electrode resistivity technique in anisotropic media: theoretical analysis and application on myocardial tissue in vivo. *IEEE Trans Biomed Eng* 40: 1138–1148, 1993.
27. **Uechi M, Asai K, Osaka M, Smith A, Sato N, Wagner TE, Ishikawa Y, Hayakawa H, Vatner DE, Shannon RP, Homcy CJ, and Vatner SF.** Depressed heart rate variability and arterial baroreflex in conscious transgenic mice with overexpression of cardiac $G_s\alpha$. *Circ Res* 82: 416–423, 1998.
28. **Uemura K, Sugimachi M, Shishido T, Kawada T, Inagaki M, Zheng C, Sato T, and Sunagawa K.** Convenient automated conductance volumetric system. *Jpn J Physiol* 52: 497–503, 2002.
29. **Uemura K, Sugimachi M, and Sunagawa K.** Self-calibratable ventricular pressure-volume telemetry system for rats (Abstract). *Circulation* 108 *Suppl* IV: IV-37, 2003.
30. **Vatner SF and Braunwald E.** Cardiovascular control mechanisms in the conscious state. *N Engl J Med* 293: 970–976, 1975.
31. **Wood JW.** Stray-capacitance neutralisation for high-resistance microelectrodes—a simple analysis. *Med Biol Eng Comput* 19: 230–236, 1981.

Annals of Biomedical Engineering, Vol. 32, No. 10, October 2004 (© 2004) pp. 1365–1383

Adaptive Predictive Control of Arterial Blood Pressure Based on a Neural Network during Acute Hypotension

KOJI KASHIHARA,[1,2] TORU KAWADA,[1] KAZUNORI UEMURA,[1] MASARU SUGIMACHI,[1] and KENJI SUNAGAWA[1]

[1]Department of Cardiovascular Dynamics, National Cardiovascular Center Research Institute, 5-7-1 Fujishirodai, Suita, Osaka 565-8565, Japan and [2]The Organization for Pharmaceutical Safety and Research, Shin-Kasumigaseki Building, 3-3-2 Kasumigaseki, Chiyoda, Tokyo 100-0013, Japan

(Received 7 August 2003; accepted 20 May 2004)

Abstract—In acute hypotension, an automated drug infusion system to control mean arterial blood pressure (MAP) has not been previously studied, though many investigations have examined the use of vasodilating drugs to control MAP in postoperative hypertension. Therefore, we examined an automated control of MAP during acute hypotension using a neural network (NN) approach. A proportional-integral-derivative (PID) control, an adaptive predictive control using a NN (APC_{NN}), a combined control of APC_{NN} and PID ($APC_{NN\text{-}PID}$), a fuzzy control, and a model predictive control were tested in computer simulation based on the MAP response to norepinephrine (NE) of 25 μg ml^{-1}. In six anesthetized rabbits, using the NE of 25 μg ml^{-1}, the PID control, APC_{NN}, and $APC_{NN\text{-}PID}$ prevented severe hypotension compared to an uncontrolled condition. Under PID control, four of the six animals showed MAP oscillation. Using NE of 50 μg ml^{-1}, the rabbits recovered from acute hypotension for all systems tested but showed sustained MAP oscillation during PID control. In conclusion, utilization of a NN for adaptive predictive control systems could facilitate the development of an automated drug infusion apparatus because it provides robust control even when acute or large perturbations and inter-individual differences in the sensitivity to therapeutic agents occur.

Keywords—Automated drug infusion system, Norepinephrine, Rabbits, Proportional-integral-derivative control.

INTRODUCTION

In a clinical setting, it is necessary to regulate many physiological parameters in the presence of disturbances including interactions among therapeutic agents, unexpected and acute changes in hemodynamic variables, and background noise.[9] Many investigators have reported on the use of automated drug infusion systems using vasodilators in postoperative hypertension[13,18,28] and multiple drug infusion systems to regulate hemodynamics such as cardiac output and mean arterial blood pressure (MAP).[9,22] However, in acute hypotension, an automated drug infusion system to control MAP has not been studied previously because no controller was robust enough to handle the associated unexpected large disturbances and complex modeling of various pathological states. If a system could be designed, which adapted to acute hypotension, and combined with a multiple drug infusion system,[9,22] it would be useful for application in a clinical setting.

Catecholamines, fluid infusion, and blood transfusion are required to maintain local circulation to vital organs during acute hypotension.[3,6,26] The catecholamines contribute to the quick recovery of MAP from a state of acute hypotension.[20,31] However, the sensitivity or responsiveness to the pharmacological agents generally differs among patients, and even within the same individual, the effects of pharmacological intervention could vary with time due to changes in a patient's underlying pathophysiology.[2] Further, the dose-response relationship is usually nonlinear, which makes a prediction of MAP response difficult. The cumulative effects of the past intervention on the current MAP[29] also complicate MAP control. Therefore, proper drug infusion for MAP control largely relies on the expertise of anesthesiologists and clinicians. Developing a reliable method for automating the drug infusion system would improve a patient's individualized drug therapy and minimize the total amount of drug required, which may allow an early tapering off of the drug.

Automated drug infusion systems for controlling MAP have been constructed previously using proportional-integral-derivative (PID) algorithms.[19,27] As long as the MAP response to pharmacological intervention does not change markedly, simple control with PID-tuned parameters works reasonably well. However, the PID controller cannot achieve maximum performance in all situations because of the nonlinear time-varying MAP response and the differences of drug sensitivity among patients.[1,13,34] To overcome the limitation of PID control, adaptive MAP controls have been developed to provide consistent

Address correspondence to Koji Kashihara, Department of Cardiovascular Dynamics, National Cardiovascular Center Research Institute, 5-7-1 Fujishirodai, Suita, Osaka 565-8565, Japan. Electronic mail: kasihara@ri.ncvc.go.jp

performance. These adaptive controllers recursively update their own parameters so as to compensate for both the time-varying characteristics of MAP response and the intra- and inter-individual differences to drug sensitivity.[18,28,33] Because the conventional adaptive controls still rely on a moment-to-moment linearity in MAP response to drug infusion, they might not be able to adapt to the nonlinear MAP response when large perturbations such as acute and severe hypotension[1] occur.

A neural network (NN) is a useful tool that can identify and learn nonlinear time-varying systems even in the presence of intra- and inter-individual variability in a patient's vital signs with large perturbations.[15,30] Therefore, an adaptive predictive control based on a NN (APC_{NN}) may be more robust compared to the conventional PID controller in stabilizing the system in the presence of nonlinearities in patient response and sensitivities to a drug.[1,11,17] The purpose of the present study was to explore the utility of a MAP control system based on an APC_{NN} algorithm. One limitation of using an advanced algorithm is that the added computational expense results in longer times for system identification compared to a simpler algorithm such as PID control. To overcome this performance limitation, we also constructed an APC_{NN} combined with PID control ($APC_{NN\text{-}PID}$). The performance of the APC_{NN} and $APC_{NN\text{-}PID}$ systems was compared to that of a traditional PID system, using a hemorrhage-induced acute hypotension condition to alter MAP. To estimate the effects of the simple adaptive control using artificial intelligence or the predictive control compared with APC_{NN} or $APC_{NN\text{-}PID}$, we tested the PID control based on fuzzy inference or model predictive control (MPC). Finally, we tested the robustness of each system, to control MAP, using two different concentrations of a vasopressor agent, norepinephrine (NE), at concentrations of 25 and 50 μg ml^{-1}.

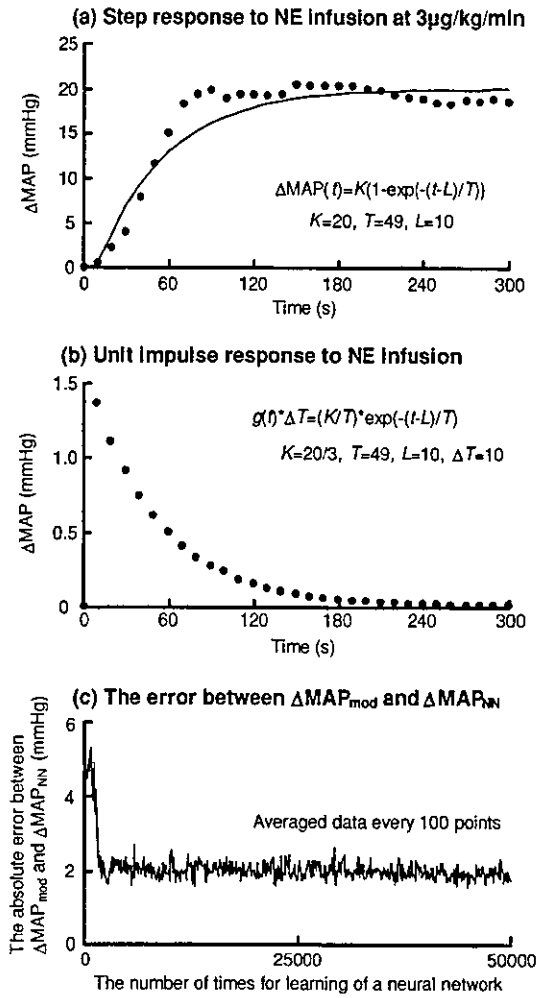

FIGURE 1. (a) Step response to norepinephrine (NE) infusion at 3 μg kg^{-1} min^{-1}, (b) Unit impulse response to NE infusion, (c) The absolute error between actual changes in mean arterial blood pressure ($\Delta MAP(t)$) as the model ($\Delta MAP_{mod}(t)$) and $\Delta MAP_{NN}(t)$ showing predicted changes in MAP by a neural network (NN).

METHODS

Modeling of MAP Response

To make a simple model for MAP response to a drug infusion, we obtained the average step response as MAP changed from baseline (ΔMAP) during a 5-min NE infusion at 3 μg kg^{-1} min^{-1} in anesthetized rabbits ($n = 3$) without hemorrhage [Fig. 1(a)]. The ΔMAP response (sampling rate = 10 Hz) was averaged every 10 s. We approximated the step response of ΔMAP to the following first-order delay system with a pure time delay:

$$\Delta MAP(t) = \begin{cases} K \cdot \left[1 - \exp\left(-\dfrac{t-L}{T}\right)\right] & (t \geq L) \\ 0 & (t < L) \end{cases} \quad (1)$$

where K is a proportional gain [mmHg (μg kg^{-1} min^{-1})$^{-1}$], T is a time constant (s), and L is the pure time delay (s). $K = 20$, $T = 49$, and $L = 10$ were acquired from the approximation of the averaged step response [Fig. 1(a)].

The ΔMAP response as a model (ΔMAP_{mod}) was calculated by the convolution integral in the discrete-time domain as follows:

$$\Delta MAP_{mod}(t) = \sum_{\tau=0}^{N_m} g(\tau) \cdot \Delta T \cdot u(t-\tau) \quad (2)$$

where

$$g(t) = \frac{K}{T} \cdot \exp\left(-\frac{t-L}{T}\right)$$

$u(t)$ is the infusion rate of NE (μg kg^{-1} min^{-1}) and $g(t)$ is the unit impulse response (mmHg). The $g(t)$ is calculated from the derivative values of the step response of Eq. (1) [Fig. 1(b)]. ΔT is the sampling interval (s) and N_m is the finite number of terms in the model for the unit impulse response.

K is a proportional gain [mmHg (μg kg^{-1} min^{-1})$^{-1}$], T is a time constant (s), and L is the pure time delay (s). The parameters of ΔMAP_{mod} were $\Delta T = 10$, $N_m = 30$, $K = 20/3$, $T = 49$, and $L = 10$.

Design of Controllers

PID Control

We applied the PID algorithm as a velocity form algorithm. The velocity form algorithm determines the drug infusion rate rather than the total amount of drug infused. The algorithm can be expressed in the discrete time domain as follows [Fig. 2(a)],[4]

$$\Delta u(t) = K_P \cdot \left\{ [e(t) - e(t-1)] + \frac{\Delta T}{T_I} \cdot e(t) + \frac{T_D}{\Delta T} \cdot [e(t) - 2 \cdot e(t-1) + e(t-2)] \right\} \quad (3)$$

$$u(t) = u(t-1) + \Delta u(t)$$

where $u(t)$ = NE infusion rate (μg kg^{-1} min^{-1}), $\Delta u(t)$ = change in $u(t)$, K_P = proportional gain [(μg kg^{-1} min^{-1}) mmHg^{-1}], T_I = integral time (s), T_D = derivative time (s), ΔT = sampling interval (10 s), $e(t)$ = difference (mmHg) between a target value and observed MAP at a given time. PID parameters were determined by the Ziegler–Nichols[36] method, resulting in $K_P = 0.3$, $T_I = 20$, and $T_D = 5$.

Adaptive Predictive Control Based on a NN (APC_{NN})

Figure 2(b) shows a block diagram of an APC_{NN} system. The APC_{NN} is a control system where the NN shown in Fig. 3 recursively learns the characteristics of a patient using their observed ΔMAP response to NE infusion, and then determines the predicted output after N_p steps. First, in the closed loop controls, the NN learned about ΔMAP response only once every 10 s to prevent overlearning of ΔMAP during rapid disturbances or artifacts ["1. Learning Loop" in Fig. 2(b) and (c)]. Second, the learned ΔMAP_{NN} response was used for the prediction of future ΔMAP responses by the NN ["2. Prediction Loop" in Fig. 2(b) and (c)]. The initial connection weights for the NN were determined from the learning-stage results using the ΔMAP_{mod} [see Eq. (2)].

Feed-Forward Output Using a NN. Figure 3 shows the components of a NN. A multilayer feed-forward NN with two hidden layers was used to emulate the ΔMAP_{mod} response. The NN structure used was a nonlinear autoregressive moving average (NARMA) model[1,32] as follows:

$$\Delta MAP_{NN}(t) = f(\Delta MAP(t-1), u(t-1), u(t-2), u(t-3), u(t-4), u(t-5), u(t-6)) \quad (4)$$

where $\Delta MAP_{NN}(t)$ is the MAP change estimated by the NN. $\Delta MAP(t-1)$ is the actual MAP change induced by NE infusion before one sampling interval (10 s) has passed. The input layer in a NN is composed of the past input and output. The duration of past NE infusion rate was set to 1 min accounting for the pure time delay in the ΔMAP response differing among patients.

The input values are sent through the first hidden layer, second hidden layer, and output layer (see Feed-Forward Output Using a NN under Appendix). When the NN calculates the output, the hyperbolic tangent function is applied 14 times (7 in the first hidden layer and 7 in the second hidden layer).

Backpropagation Algorithm for Learning. To identify the MAP response and determine the initial weights in a NN for MAP controls, the NN was trained using the output of the ΔMAP_{mod} response to random inputs. In the present study, we used the backpropagation algorithm in the online mode as follows.

All connection weights are adjusted to decrease the error function by the backpropagation learning rule based on the gradient descent method.[24,25] The error function, E is as follows:

$$E = \frac{1}{2} \cdot \varepsilon^2 = \frac{1}{2} \cdot [\Delta MAP - \Delta MAP_{NN}]^2 \quad (5)$$

where ΔMAP is the actual MAP change as a supervised signal, ΔMAP_{NN} is the ΔMAP predicted by the NN before update of the connection weights, and ε is the difference between ΔMAP and ΔMAP_{NN}. The ΔMAP_{NN} predicted by a NN is compared with the actual ΔMAP, and its error is calculated by Eq. (5). The error is back propagated through the network, and the connection weight is generally updated by the gradient descent of E as a function of the weights.[30]

$$w^* = w + Kn \cdot \Delta w \quad (6)$$

where

$$\Delta w = \frac{\partial E}{\partial w} = \frac{\partial E}{\partial \varepsilon} \cdot \frac{\partial \varepsilon}{\partial MAP_{NN}} \cdot \frac{\partial MAP_{NN}}{\partial w} = -\varepsilon \cdot \frac{\partial MAP_{NN}}{\partial w},$$

w^* is the weight of each connection after update, w is the weight of each connection before update, Δw is the modified weight, K_n is the learning rate.

In the present study, the backpropagation algorithm was performed in the following order: output layer, second hidden layer, and first hidden layer (see Backpropagation Algorithm for Learning under Appendix). The total number of weights in the NN was 120 (105 for layer weights and 15 for bias, Fig. 3). The combination of a fixed input $x_0 = 1$ and an extra input weight w_0 is known as a bias input (Fig. 3[1,30]).

Determination of Initial Weights in a NN. To determine the initial weights in the NN for the APC_{NN} and $APC_{NN\text{-}PID}$, we made the NN learn the ΔMAP_{mod} response. The starting

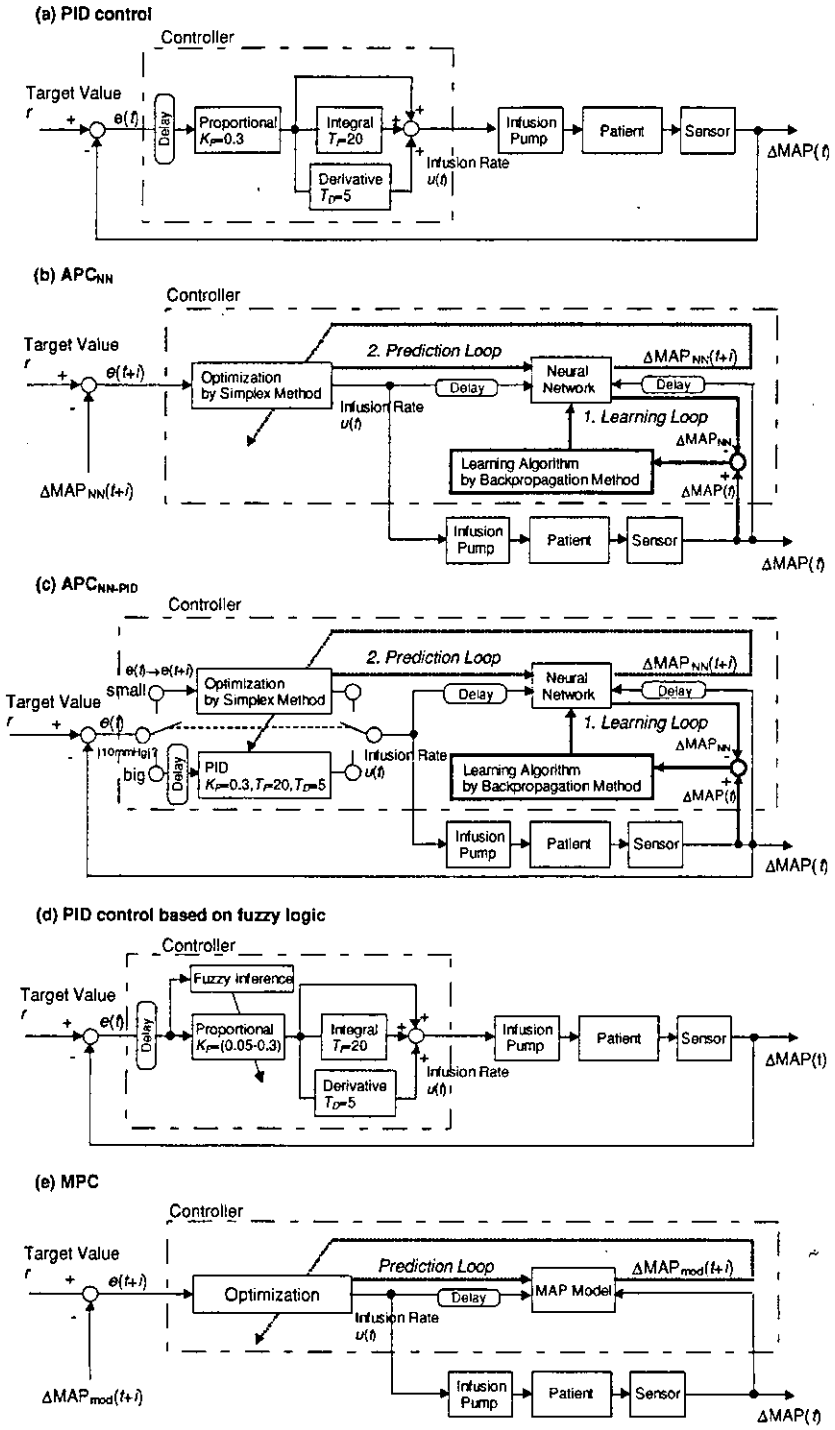

FIGURE 2. The block diagram for a MAP control system. (a) A proportional-integral-derivative (PID) control. (b) An adaptive predictive control using a neural network (APC$_{NN}$). (c) APC$_{NN}$ combined with PID control (APC$_{NN-PID}$). (d) PID control based on fuzzy inference. (e) Model predictive control (MPC). $u(t)$: infusion rate of NE. r: a target value. $e(t)$: error between the target value and observed MAP. $e(t+i)$: error between the target value and MAP predicted by the NN ($\Delta MAP_{NN}(t+i)$) or the model MAP response ($\Delta MAP_{mod}(t+i)$). $\Delta MAP(t)$, ΔMAP_{NN}, and $\Delta MAP_{NN}(t+i)$ are actual changes in MAP, MAP changes by the NN before update, and changes in MAP predicted by the NN, respectively.